

# Accuracy and stiffness analysis of a 3-RRP spherical parallel manipulator

Javad Enferadi†\* and Alireza Akbarzadeh Tootoonchi‡

†Department of Mechanical Engineering, Ferdowsi University of Mashhad, Mashhad, Iran

‡Department of Mechanical Engineering, Ferdowsi University of Mashhad, Mashhad, Iran

(Received in Final Form: January 11, 2010. First published online: March 4, 2010)

## SUMMARY

In this paper, accuracy and stiffness analysis of a 3-RRP spherical parallel manipulator (SPM) (Enferadi and Tootoonchi, A novel spherical parallel manipulator: Forward position problem, singularity analysis and isotropy design, *Robotica*, vol. 27, 2009, pp. 663–676) with symmetrical geometry is investigated. At first, the 3-RRP SPM is introduced and its inverse kinematics analysis is performed. Isotropic design, because of its design superiority, is selected and workspace of the manipulator is obtained. The kinematics conditioning index (KCI) is evaluated on the workspace. Global conditioning index (GCI) of the manipulator is calculated and compared with another SPM. Unlike traditional stiffness analysis, the moving platform is assumed to be flexible. A continuous method is used for obtaining mathematical model of the manipulator stiffness matrix. This method is based on strain energy and Castigliano's theorem. The mathematical model is verified by finite element model. Finally, using mathematical model, kinematics stiffness index (KSI), and global stiffness index (GSI) are evaluated.

**KEYWORDS:** Spherical parallel manipulator, Inverse kinematics, Accuracy analysis, Stiffness analysis, Finite element method.

## 1. Introduction

A parallel manipulator typically consists of a moving platform and a fixed base that are connected together by several limbs. Because of the closed-loop architecture, not all joints can be independently actuated. In general, the number of actuated joints is equal to the number of degrees of freedom of the manipulator. A spherical parallel manipulator (SPM) is one in which the end-effector is moved on the surface of a sphere. In other words, the end-effector can rotate around any axis passing through a fixed point, center of sphere. Thus, all points fixed to the moving platform move on concentric spheres.<sup>2</sup> Therefore, a spherical manipulator can be used as a device to orient the end-effector. Spherical manipulators can be either serial<sup>3</sup> or parallel.<sup>2,4–5</sup> Parallel architectures are usually more stiff and accurate than the serial ones; however, their structures are more complex.

Accuracy of Parallel manipulators is of utmost importance. Therefore, simple and fast methods for computing the accuracy of a given robot design are needed. This information can then be used in design optimization procedures that look for maximum accuracy. Accuracy errors in position and orientation of a parallel robot are due to several factors, among them:

- Manufacturing errors, which may be taken into account through calibration.
- Preloading, backlash, and other mechanical clearances, which may be minimized through proper choice of mechanical components.
- Compliance, which may be minimized through the use of more rigid structures and proper choice of material (though these may increase inertia and decrease operating speed).
- Actuated joints errors, coming from the finite resolution of motor encoders.
- Control errors coming from inaccurate mechanical and electrical dynamic models and sensor errors.
- Round off errors mainly coming from calculating inverse of Jacobian matrix. Structural design and configuration effect Jacobian matrix. Therefore, these errors can be minimized by choosing an isotropic design and avoiding workspace singularities.

Parallel manipulator design can be based on many criteria such as, workspace,<sup>6–7</sup> dexterity,<sup>8–9</sup> payload,<sup>10</sup> global conditioning index (GCI),<sup>11–13</sup> stiffness<sup>14</sup> and singularity avoidance.<sup>15</sup> Depending on the application each of these criteria may be emphasized by the robot designer. For example, stiffness and GCI may be more important in an application where a parallel manipulator is used to orient material for computer numerical control (CNC) machine tool. Several performance indices have been developed and used to roughly evaluate the accuracy of serial and parallel robots. An exhaustive study<sup>16</sup> reviewed most of these performance indices and discussed their inconsistencies when applied to parallel robots with having both translational and rotational degrees of freedom.

The most common performance indices used to indirectly optimize the accuracy of parallel robots are the dexterity index<sup>9</sup> and the GCI.<sup>17</sup>

In theory, parallel mechanisms seem capable of answering the increasing needs of industry in terms of automation.

\* Corresponding author. E-mail: Javadenferadi@gmail.com

The nature of their architectures tends to reduce absolute positioning and orienting errors.<sup>18</sup> Furthermore, since the actuators of a parallel mechanism are often fixed to its base, the inertia of its mobile parts is reduced and the end-effector can perform movements with higher accelerations. These factors have led to an increase in parallel mechanism's popularity. Another important characteristic of parallel manipulators is high stiffness. Stiffness is a mechanical characteristic, which describes the behavior of a structure under static force in terms of elastic deflection. It can be evaluated for robotic manipulators by means of specific formulation and experimental tests.<sup>19</sup> When a manipulator performs a given task, the end-effector exerts force and/or moment onto its environment. The reaction force and/or moment will cause the end-effector to be deflected away from its desired location. Intuitively, the amount of deflection is a function of the applied force and/or moment and the stiffness of the manipulator. Thus, the stiffness of a manipulator is related with accurate positioning and high payload capability. A simple way to predict the stiffness of a manipulator is to obtain its stiffness matrix.<sup>20</sup> Additionally, stiffness can be evaluated using the eigenvalues of the stiffness matrix which is experienced in the direction of the corresponding eigenvectors.<sup>14,21</sup> It has been shown that the stiffness is bounded by the minimum and maximum eigenvalues of the stiffness matrix.<sup>22</sup> Therefore, stiffness values have been reported by evaluating either minimum, maximum, average eigenvalues and/or ratio of the maximum and minimum eigenvalues of the stiffness matrix.<sup>22</sup> Additionally, the determinant of stiffness matrix, which is the product of its eigenvalues, has been adopted to assess the stiffness of parallel manipulators.<sup>19,23</sup>

Condition number of the stiffness matrix may also be calculated in the same manner that the condition number of Jacobian matrix is calculated. The global stiffness index (GSI) can now be defined as the inverse of the condition number of the stiffness matrix integrated over the reachable workspace divided by the workspace volume.<sup>24</sup>

In the present paper, accuracy, and stiffness analysis of an SPM with symmetric geometry is investigated. First, the SPM namely spherical star triangle (SST) is re-introduced. The forward kinematics problem, isotropic design, and singularity analysis of this manipulator has been previously investigated and reported in ref. [1]. We select the isotropic design because it is the superior design and obtain its performance indices. Although the isotropic design is selected, all methods presented in this paper apply to general structure of SST manipulator. To perform accuracy and stiffness analysis, the inverse kinematics problem is first solved. Next, workspace of the manipulator is obtained and its kinematics accuracy is evaluated on its workspace. GCI of the manipulator is calculated and compared with another parallel manipulators with known GCI. It is shown that the SST manipulator has relatively high accuracy. Unlike traditional parallel manipulators that used a plate as moving platform, the moving platform of SST manipulator is constructed by three branches or rods. It is then natural to consider the flexibility of these three branches. Therefore, the moving platform is considered flexible and a continuous model is used for its representation. To the

best of authors' knowledge previous work in this area have assumed a rigid moving platform and a lumped model.<sup>25–26</sup> Next, using strain energy the mathematical model relating stiffness and end-effector deflection is developed. Using commercial software, a finite element model for end-effector rotation is also developed. The results of the mathematical and finite element models for several configurations on the workspace are compared. It is shown that the two models are in close agreement. Finally, using mathematical model, the kinematics stiffness index (KSI) and GSI are evaluated.

## 2. Description of the Spherical Star Triangle Parallel Manipulator

The SST parallel manipulator consists of a fixed spherical triangular base  $P$  and a moving platform which is shaped like a spherical star  $S$ . The fixed base and the moving platform are connected via three legs. Each of the three moving legs is made of curved prismatic-revolute-curved prismatic (PRP) joints. We use the term curved prismatic to denote a motion that slides on a curved path. An example of this joint used in industry is CURVILINE which is a curved linear bearing.<sup>27</sup> The three branches of the spherical star and the three moving legs are each assumed to be identical resulting in a symmetrical geometry for the SST manipulator. The general model of this manipulator is depicted in Fig. 1. The first curved prismatic joint which is also the motorized joint moves along circular arc,  $P_1P_{i+1}$ , located on the surface of the sphere. In practice, it is difficult to manufacture an actuated curved prismatic joint which moves on a circular arc. However, by closer inspection, one can see that each of the motorized joints can also be viewed as a revolute joint with its axis passing through the origin of the sphere (see Figs. 2 and 3). Another word, each of the three legs can also be thought of being revolute-revolute-curved prismatic (RRP) joints. Therefore, to physically construct this manipulator we will build its legs with RRP joints. The physical model

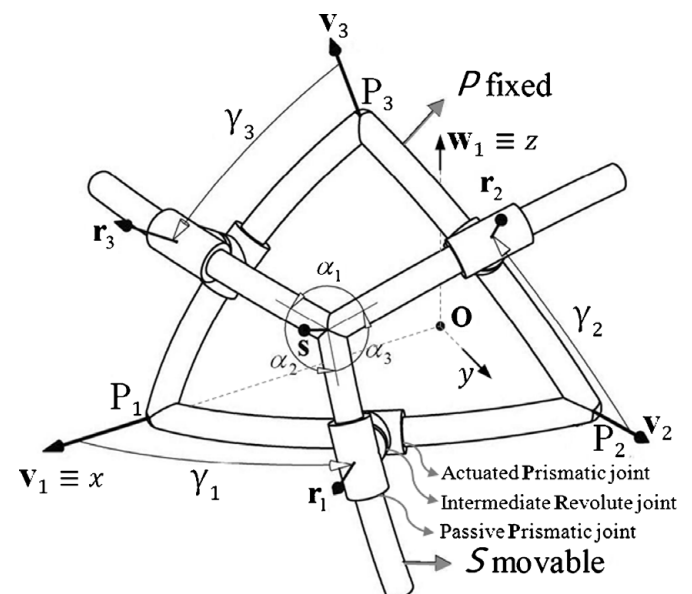


Fig. 1. General model of SST.

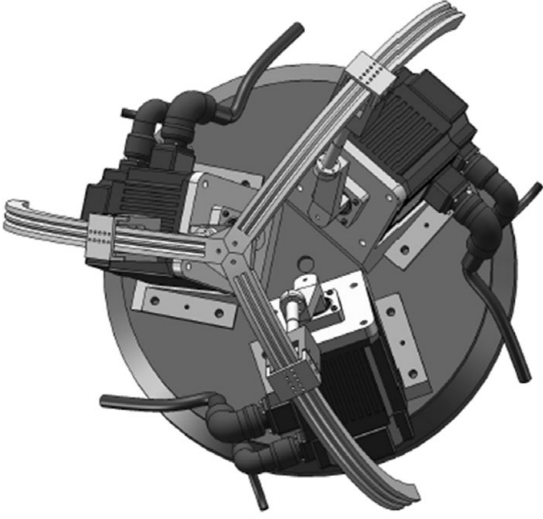
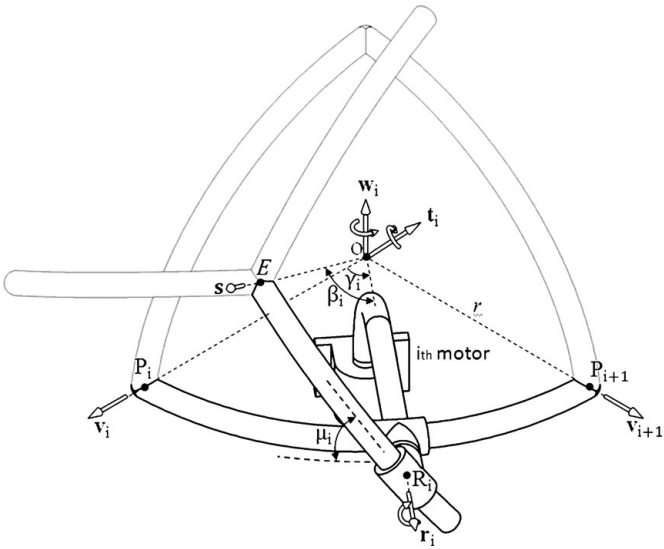


Fig. 2. Physical model of the SST manipulator with motors.


 Fig. 3. Parameters description of  $i$ th leg.

of this manipulator is depicted in Fig. 2. To develop the mathematical model of the manipulator, first a sphere with center at  $O$  and a fixed spherical triangle,  $P_1P_2P_3$ , on its surface is considered. The unit vector  $\mathbf{v}_i$  is defined along  $OP_i$ .

$$\mathbf{}^B_E\mathbf{R} = \begin{bmatrix} \cos \theta \cos \varphi \cos \psi - \sin \theta \sin \psi & -\cos \theta \cos \varphi \sin \psi - \sin \theta \cos \psi & \cos \theta \sin \varphi \\ \sin \theta \cos \varphi \cos \psi + \cos \theta \sin \psi & -\sin \theta \cos \varphi \sin \psi + \cos \theta \cos \psi & \sin \theta \sin \varphi \\ -\sin \varphi \cos \psi & \sin \varphi \sin \psi & \cos \varphi \end{bmatrix}, \quad (3)$$

Actuators stroke which can travel along the arc  $P_iP_{i+1}$  are defined by angle  $\gamma_i$  (see Figs. 1 and 3). The moving spherical star (MSS),  $S$ , is next considered. The star is made of three arcs which are located on a surface of a second sphere. The first and the second sphere have the same center but the radius of the second sphere is slightly larger due to intermediate

revolute joint. This difference should be minimized in order to increase the structural stiffness of the manipulator. The three arcs of MSS intersect at point  $E$ . The angle between these arcs,  $\alpha_1$ ,  $\alpha_2$ , and  $\alpha_3$  can be manually selected by the robot designer to obtain the desired performance. Position of point  $E$  defines end-effector position. Direction  $OE$  can be defined by unit vector  $\mathbf{s}$  (see Figs. 1 and 3). The arcs of the moveable star platform  $ER_i$  intersect the line which is along actuator links at the point  $R_i$ . Angular position of the actuators are defined by the unit vector  $\mathbf{r}_i$ . Direction of this unit vector is defined along  $OR_i$ . Furthermore,  $R_i$  is a joint which allows rotation about  $\mathbf{r}_i$  axis as well as a rotation about the axis that passes through center of sphere,  $O$  and is perpendicular to  $OER_i$  plane (see Fig. 3).

### 3. Unit Vectors and Coordinates Frames

In this section, we define unit vectors and two coordinate frames that are required to solve inverse kinematic problem and perform velocity analysis of SST manipulator. For this purpose, two unit vectors  $\mathbf{t}_i$  and  $\mathbf{w}_i$  are defined as follows:

$$\mathbf{t}_i = \frac{\mathbf{s} \times \mathbf{r}_i}{\|\mathbf{s} \times \mathbf{r}_i\|}, \quad (1)$$

$$\mathbf{w}_i = \frac{\mathbf{v}_i \times \mathbf{v}_{i+1}}{\|\mathbf{v}_i \times \mathbf{v}_{i+1}\|}, \quad (2)$$

where the unit vectors  $\mathbf{t}_i$  and  $\mathbf{w}_i$  are perpendicular to planes  $OER_i$  and  $OP_iP_{i+1}$ , respectively (See Fig. 3). The first coordinate frame  $\mathbf{B}(x, y, z)$  is attached to the fixed base and is called base coordinate frame. The  $x$  and  $z$  axes of this frame are chosen along the unit vectors  $\mathbf{v}_1$  and  $\mathbf{w}_1$  respectively (see Figs. 4 and 5(a)). The  $y$  axis is chosen by the right hand rule. The second coordinate frame  $\mathbf{E}(u, v, w)$  is attached to the MSS and is called the moving coordinate frame. The  $v$  and  $w$  axes of this frame are chosen along  $\mathbf{t}_i$  and  $\mathbf{s}$ , respectively (see Figs. 4 and 5(d)). The  $u$  axis is chosen by the right hand rule. The coordinate frames as well as unit vectors defined will now allow us to describe the MSS rotation with respect to the fixed base. Using  $w$ - $v$ - $w$  Euler angles, the rotation matrix is defined as

where angles  $\theta$ ,  $\varphi$ , and  $\psi$  specify the MSS orientation. Angle  $\theta$  is rotation about  $z$  axis, angle  $\varphi$  is rotation about  $y'$  axis and angle  $\psi$  is rotation about  $z''$  axis. These rotations are shown in Fig. 5. The moving coordinate frame  $\mathbf{E}(u, v, w)$  is shown in Fig. 5(d) and coincides with coordinate frame  $(x''', y''', z''')$ .

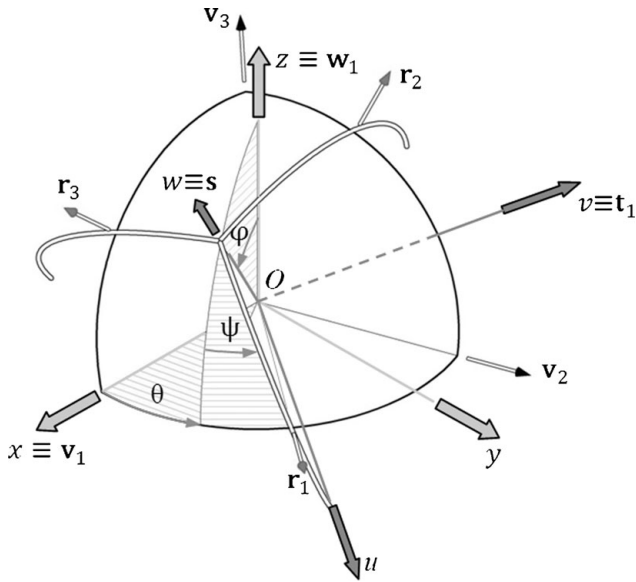


Fig. 4. The fixed coordinate frame, the moving coordinate frame, and orientation of MSS.

**4. Inverse Kinematics Analysis**

A solution to the inverse kinematics problem is required for accuracy and stiffness analysis. Therefore, inverse

kinematics problem of SST manipulator is the subject of this section. The orientation of the MSS is defined by unit vector  $s$  as well as angle  $\psi$  (the rotation angle about the unit vector  $s$ ) according to Figs. 4 and 5(d). The unit vector  $s$  is defined by two angles  $\theta$  and  $\varphi$ . Therefore, the orientation analysis (inverse kinematics problem) can be defined as: given orientation of the MSS (unit vector  $s$  and angle  $\psi$ ) and other kinematics parameters, obtain the actuator rotations,  $\gamma_i$ .

For inverse kinematics analysis, we use equivalent angle-axis representation<sup>28–29</sup> which is special form of Rodriguez formula.<sup>30</sup> The equivalent angle-axis representation is defined by

$$Q(\mathbf{e}, \eta) = \cos \eta \mathbf{I}_{3 \times 3} + (1 - \cos \eta) \mathbf{e} \mathbf{e}^T + \sin \eta \begin{bmatrix} 0 & -e_z & e_y \\ e_z & 0 & -e_x \\ -e_y & e_x & 0 \end{bmatrix}, \quad (4)$$

where the unit vector  $\mathbf{e}$  is the axis of rotation,  $\eta$  is the angle of rotation about the unit vector  $\mathbf{e}$ , and  $e_x, e_y, e_z$  are Cartesian components of the unit vector  $\mathbf{e}$ .

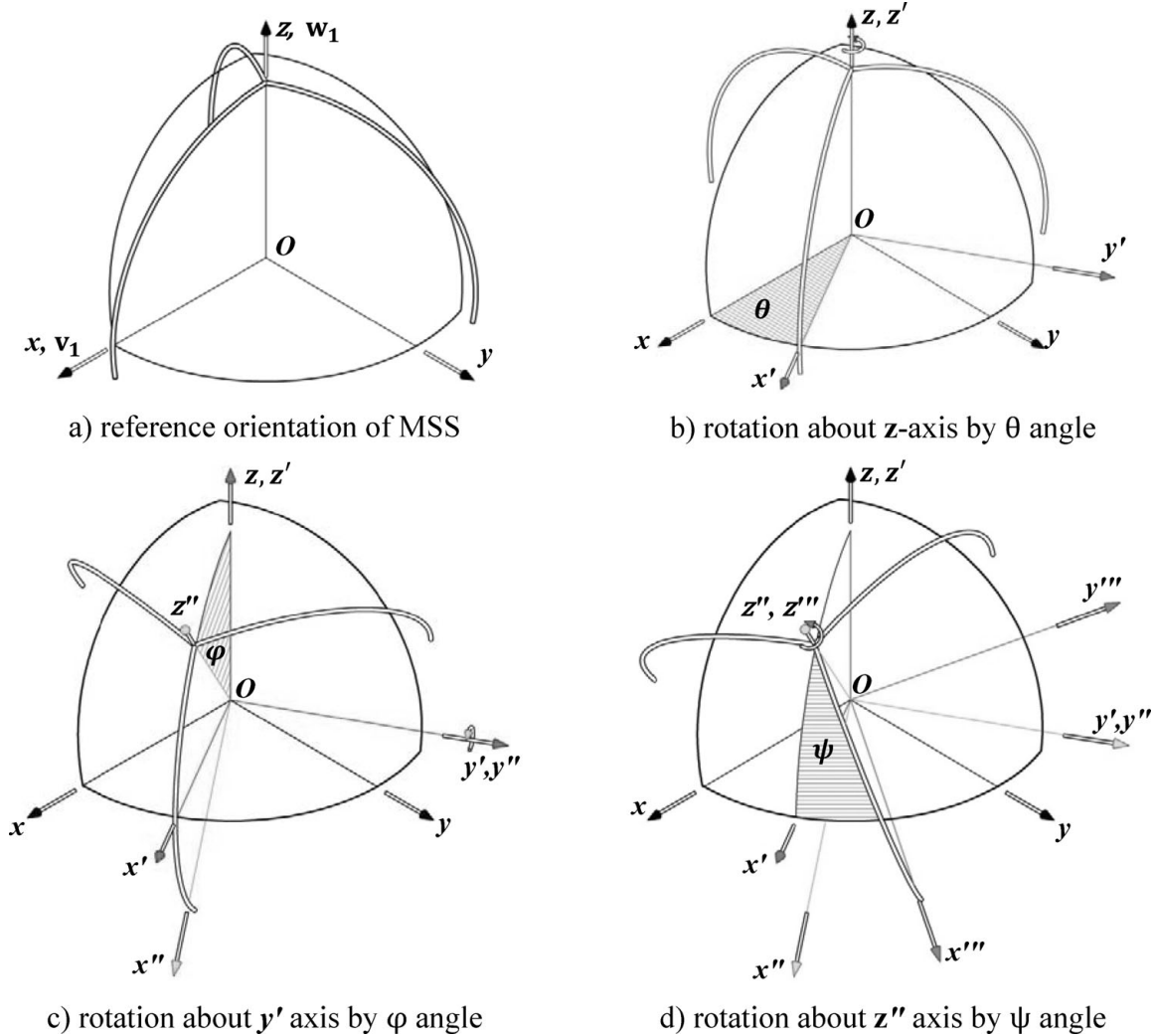


Fig. 5. Rotation angles of MSS with respect to the base coordinate frame.

The step by step procedure for solving inverse kinematics problem of the SST manipulator is as follow:

**Step 1:** Given rotation matrix MSS with respect to base frame,  ${}^B_E\mathbf{R}$ , unit vectors  $\mathbf{s}$  and  $\mathbf{t}_1$  can be calculated.

As stated before, the  $\mathbf{w}$  and  $\mathbf{v}$  axes of the base coordinate frame  $\{B\}$  are along the unit vectors  $\mathbf{s}$  and  $\mathbf{t}_1$ , respectively (See Fig. 4). Therefore, we can write  $\mathbf{s}$  and  $\mathbf{t}_1$  in the base coordinate frame as follows:

$$\mathbf{s} = {}^B_E\mathbf{R}^E\mathbf{w} = {}^B_E\mathbf{R} \begin{bmatrix} 0 \\ 0 \\ 1 \end{bmatrix} = \begin{bmatrix} \cos\theta \sin\varphi \\ \sin\theta \sin\varphi \\ \cos\varphi \end{bmatrix}, \quad (5)$$

$$\begin{aligned} \mathbf{t}_1 &= {}^B_E\mathbf{R}^E\mathbf{v} = {}^B_E\mathbf{R} \begin{bmatrix} 0 \\ 1 \\ 0 \end{bmatrix} \\ &= \begin{bmatrix} -\cos\theta \cos\varphi \sin\psi - \sin\theta \cos\psi \\ -\sin\theta \cos\varphi \sin\psi + \cos\theta \cos\psi \\ \sin\varphi \sin\psi \end{bmatrix}. \end{aligned} \quad (6)$$

**Step 2:** Using equivalent axis-angle representation, we can define unit vectors  $\mathbf{t}_2$  and  $\mathbf{t}_3$ .

The physical structure of the moveable star can be used in order to find unit vectors  $\mathbf{t}_2$  and  $\mathbf{t}_3$  (consider Fig. 3). The unit vector,  $\mathbf{t}_i$ , is perpendicular to the plane that contains the corresponding arc,  $ER_i$ , of the moveable star. We previously obtained  $\mathbf{t}_1$  in step 1. Now, using Eq. (4), the unit vectors  $\mathbf{t}_2$  and  $\mathbf{t}_3$  can be obtained by rotating  $\mathbf{t}_1$  about  $\mathbf{s}$  by  $\alpha_3$  and  $-\alpha_2$ , respectively:

$$\begin{aligned} \mathbf{t}_2 &= \mathbf{Q}(\mathbf{s}, \alpha_3)\mathbf{t}_1 = \cos\alpha_3\mathbf{I}_{3\times3}\mathbf{t}_1 \\ &\quad + (1 - \cos\alpha_3)\mathbf{ss}^T\mathbf{t}_1 + \sin\alpha_3(\mathbf{s} \times \mathbf{t}_1), \end{aligned} \quad (7)$$

$$\begin{aligned} \mathbf{t}_3 &= \mathbf{Q}(\mathbf{s}, -\alpha_2)\mathbf{t}_1 = \cos\alpha_2\mathbf{I}_{3\times3}\mathbf{t}_1 \\ &\quad + (1 - \cos\alpha_2)\mathbf{ss}^T\mathbf{t}_1 - \sin\alpha_2(\mathbf{s} \times \mathbf{t}_1). \end{aligned} \quad (8)$$

The unit vector  $\mathbf{t}_i$  is perpendicular to the unit vector  $\mathbf{s}$ . Therefore, above equations can be simplified as,

$$\mathbf{t}_2 = \cos\alpha_3\mathbf{t}_1 + \sin\alpha_3(\mathbf{s} \times \mathbf{t}_1), \quad (9)$$

$$\mathbf{t}_3 = \cos\alpha_2\mathbf{t}_1 - \sin\alpha_2(\mathbf{s} \times \mathbf{t}_1). \quad (10)$$

**Step 3:** Position of the actuators are described by unit vectors  $\mathbf{r}_i$  as a function of  $\gamma_i$  for  $i = 1, 2, 3$ .

Consider Figs. 1 and 3. The three actuated curved prismatic joints move along arc  $P_iP_{i+1}$ . This motion can be viewed as revolution about an axis that passes through the origin of the sphere. This axis is defined by a unit vector,  $\mathbf{w}_i$ . This unit vector is perpendicular to the plane  $OP_iP_{i+1}$  and passes through origin. In inverse kinematics problem, positions of the actuators are unknown. These positions are defined by the unit vectors  $\mathbf{r}_i$ . The unit vector can be defined by rotation of unit vector  $\mathbf{v}_i$  about unit vector  $\mathbf{w}_i$  in positive direction by angle  $\gamma_i$ . Therefore, unit vector  $\mathbf{r}_i$  can be written

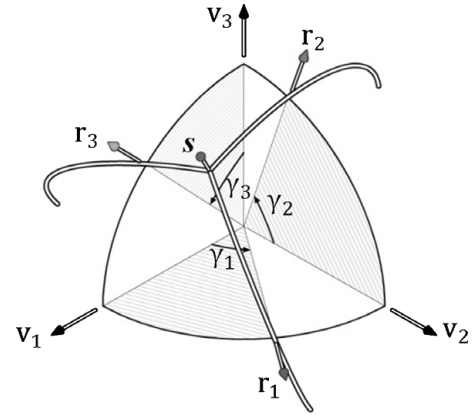


Fig. 6. Rotation value of actuators.

as

$$\begin{aligned} \mathbf{r}_i &= \mathbf{Q}(\mathbf{w}_i, \gamma_i)\mathbf{v}_i \\ &= \cos\gamma_i\mathbf{I}_{3\times3}\mathbf{v}_i + (1 - \cos\gamma_i)\mathbf{w}_i\mathbf{w}_i^T\mathbf{v}_i \\ &\quad + \sin\gamma_i(\mathbf{w}_i \times \mathbf{v}_i). \end{aligned} \quad (11)$$

Since  $\mathbf{v}_i$  is perpendicular to  $\mathbf{w}_i$ , the above equation can be simplified as

$$\mathbf{r}_i = \cos\gamma_i\mathbf{v}_i + \sin\gamma_i(\mathbf{w}_i \times \mathbf{v}_i) \quad \text{for } i = 1, 2, 3. \quad (12)$$

Therefore the unit vector  $\mathbf{r}_i$  is defined as a function of unknown angle  $\gamma_i$ .

**Step 4:** Obtaining rotation angle of the actuators,  $\gamma_i$ .

To obtain unknown angles  $\gamma_i$ , three independent trigonometric equations are formulated by noting that  $\mathbf{t}_i$  is perpendicular to  $\mathbf{r}_i$  (see Eq. (1)):

$$\mathbf{r}_i^T\mathbf{t}_i = 0 \quad \text{for } i = 1, 2, 3. \quad (13)$$

Equations (6), (9), (10), and (12) can be placed in Eq. (13) which results in

$$\cos\gamma_i\mathbf{v}_i^T\mathbf{t}_i + \sin\gamma_i(\mathbf{w}_i \times \mathbf{v}_i)^T\mathbf{t}_i = 0 \quad \text{for } i = 1, 2, 3. \quad (14)$$

Therefore, closed form solution of inverse kinematics problem is given by

$$\gamma_i = A \tan 2[-\mathbf{v}_i^T\mathbf{t}_i, (\mathbf{w}_i \times \mathbf{v}_i)^T\mathbf{t}_i] \quad \text{for } i = 1, 2, 3. \quad (15)$$

Note that  $\mathbf{v}_i^T\mathbf{t}_i$  and  $(\mathbf{w}_i \times \mathbf{v}_i)^T\mathbf{t}_i$  both have numerical values. This is because,  $\mathbf{t}_i$  were calculated in steps 1 and 2,  $\mathbf{v}_i$  are known and given by the structure of the base spherical triangle, and  $\mathbf{w}_i$  are obtained by Eq. (2). The angles  $\gamma_i$  representing rotational values of actuators are shown in Fig. 6. This completes solution of inverse kinematics problem.

Now, we can obtain the unit vectors  $\mathbf{r}_i$  using of Eq. (12). These unit vectors are needed to obtain Jacobian matrices, workspace, accuracy analysis and stiffness analysis of the SST manipulator. Also, we can calculate the  $\beta_i$  angles as follows:

$$\beta_i = \cos^{-1}(\mathbf{r}_i^T\mathbf{s}). \quad (16)$$

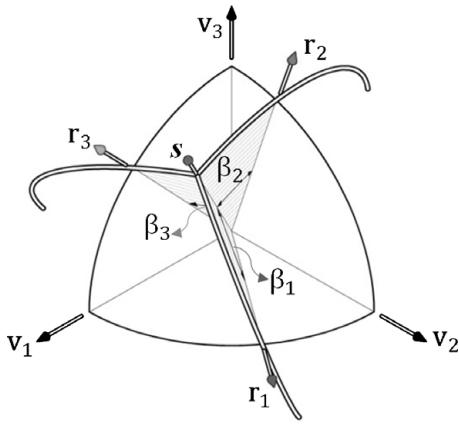


Fig. 7. The angles  $\beta_i$ .

The angles  $\beta_i$  are shown in Fig. 7 and will be later needed for stiffness analysis of the SST manipulator.

**5. Kinematics Accuracy Analysis**

The structure of SST manipulator can be designed as either isotropic or non-isotropic. The isotropic design of this manipulator has several advantages. For example, it has a relatively a large workspace since the end-effector can travel the entire area of its fixed spherical triangle base. Additionally, all points in the workspace are free of singularities.<sup>1</sup> Therefore, the isotropic design is considered for the kinematics accuracy analysis. To perform the accuracy analysis, kinematics and global conditioning indices must be determined. These two indices require the knowledge of condition numbers of Jacobian matrices.

*5.1. Jacobian matrices*

For parallel mechanisms in general, the Jacobian matrix is used to establish a relation between generalized and actuators velocities as well as between generalized and actuators forces and couples. This relation for SST manipulator can be written as,

$$\mathbf{J}_1 \dot{\boldsymbol{\gamma}} + \mathbf{J}_2 \boldsymbol{\omega} = \mathbf{0}. \tag{17}$$

where  $\mathbf{J}_1$  and  $\mathbf{J}_2$  are the direct kinematic problem and inverse kinematic problem Jacobian matrices for the SST manipulator, respectively. Moreover,  $\dot{\boldsymbol{\gamma}}$  is the vector of actuated joint rates and  $\boldsymbol{\omega}$  is the angular velocity of the moving platform, MSS, defined in the base frame. The Jacobian matrices  $\mathbf{J}_1$  and  $\mathbf{J}_2$  are obtained by velocity analysis and reported in ref.<sup>1</sup> as follows:

$$\mathbf{J}_1 = \begin{bmatrix} c_1 & 0 & 0 \\ 0 & c_2 & 0 \\ 0 & 0 & c_3 \end{bmatrix} \tag{18}$$

and

$$\mathbf{J}_2 = \begin{bmatrix} -(\mathbf{r}_1 \times \mathbf{t}_1)^T \\ -(\mathbf{r}_2 \times \mathbf{t}_2)^T \\ -(\mathbf{r}_3 \times \mathbf{t}_3)^T \end{bmatrix}, \tag{19}$$

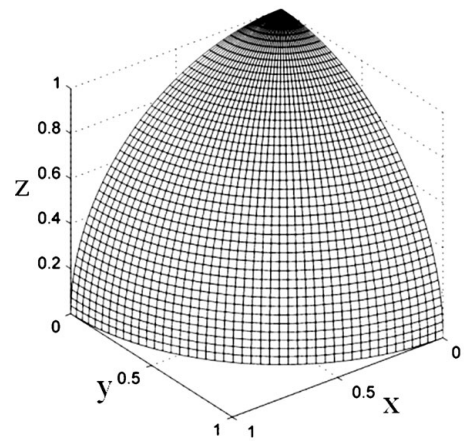


Fig. 8. Discreted area of the fixed base spherical triangle.

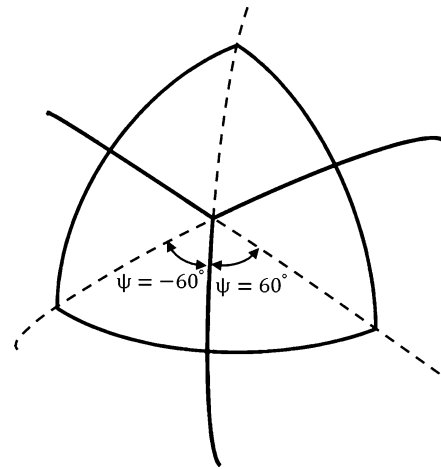


Fig. 9. Range of values for  $\psi$ .

where

$$c_i = (\mathbf{r}_i \times \mathbf{t}_i)^T \mathbf{w}_i \quad \text{for } i = 1, 2, 3. \tag{20}$$

Equation (17) may be used to obtain a single Jacobian matrix for the manipulator

$$\mathbf{J} \dot{\boldsymbol{\gamma}} = \boldsymbol{\omega}, \tag{21}$$

Where  $\mathbf{J} = -\mathbf{J}_2^{-1} \mathbf{J}_1$ .

*5.2. Workspace determination*

Robot workspace is an important criterion in evaluating manipulator performance. Determination of the workspace can be performed either by a numerical discretization of the Cartesian space or by the derivation of analytical expressions of the boundaries of the workspace.<sup>31-32</sup>

In this paper, we use the first method and determine workspace of isotropic design of the SST manipulator. To perform workspace analysis, we will assume the radius of the sphere is unity (for example, one meter). To determine workspace, we discretize area of the base spherical triangle according to Fig. 8. Next, we move end-effector on the discretized area for different values of angle  $\psi$ . According to Fig. 4, for the isotropic design, range of values for  $\theta$  and  $\varphi$  is  $0^\circ$  to  $90^\circ$ . Similarly according to Fig. 9, for the isotropic design, the range of values for  $\psi$  is  $-60^\circ$  to  $60^\circ$ . The following procedure determines the workspace.

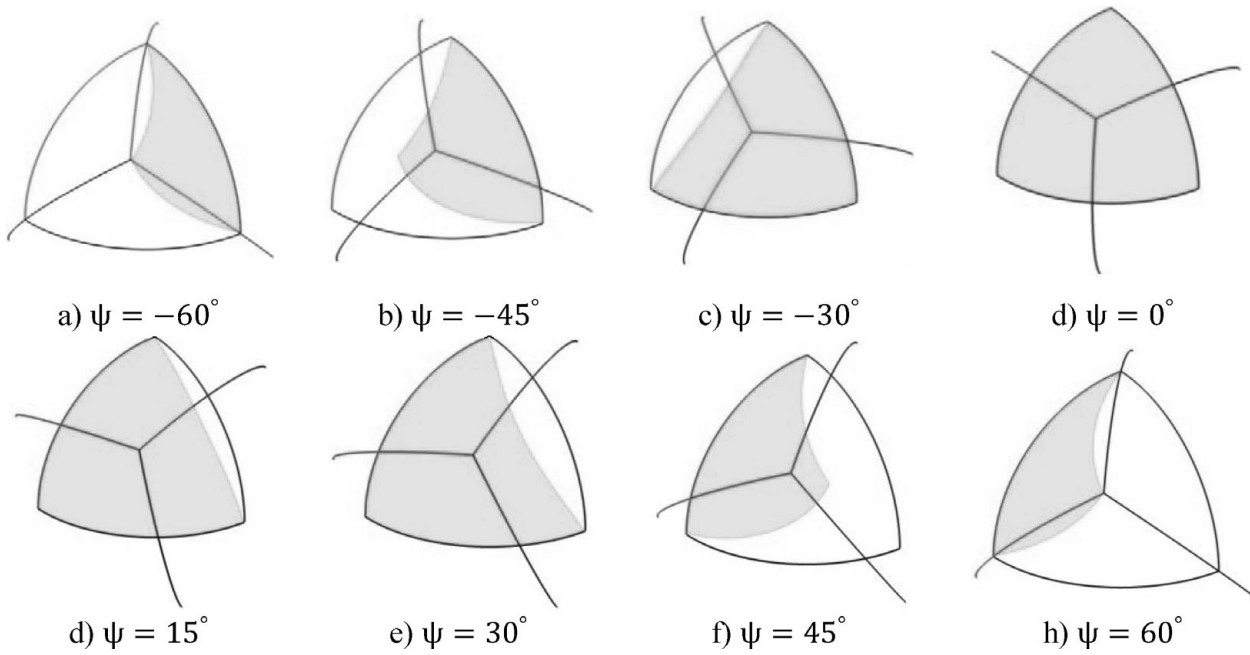


Fig. 10. Workspace area of the SST manipulator on sphere in x-y-z space for different  $\psi$ .

---

```

For  $\psi = -60^\circ$  to  $60^\circ$ 
  For  $\theta = 0^\circ$  to  $90^\circ$ 
    For  $\phi = 0^\circ$  to  $90^\circ$ 
      Calculate  $\gamma_i$  using Eq. (15)
      If  $0^\circ \leq \gamma_i \leq 90^\circ$  Then
        Point on sphere is on workspace
      Else
        Point is not on workspace
    Next  $\phi$ 
  Next  $\theta$ 
Next  $\psi$ 
    
```

---

As shown in Fig. 10, workspace of the SST manipulator depends on the angle  $\psi$ . This figure shows that workspace for  $\psi = -60^\circ$  and  $\psi = 60^\circ$  is minimum and is maximum for  $\psi = 0^\circ$ .

The volumetric workspace in  $\theta$ - $\phi$ - $\psi$  space is shown in Fig. 11. Area of the workspace, on the sphere, for different values of  $\psi$  is calculated and shown in Fig. 12. The maximum workspace area occurs at  $\psi = 0^\circ$  and its value is equal to 1.57 square units. This value represents one-eighth area of a sphere with radius of unity (see Fig. 10d). This value is equal to the area of fixed base spherical triangle and shows that end-effector can travel the entire area of its base. Therefore, SST manipulator has a relatively large workspace.

In the next sections, we will use workspace of the manipulator to perform kinematics accuracy analysis as well as stiffness analysis.

### 5.3. Kinematics accuracy analysis

As shown by Strang,<sup>33</sup> condition number is a measure of stability or sensitivity of a matrix to numerical operations. It is used in numerical analysis to estimate the error generated in the solution of a linear system of equations. In numerical

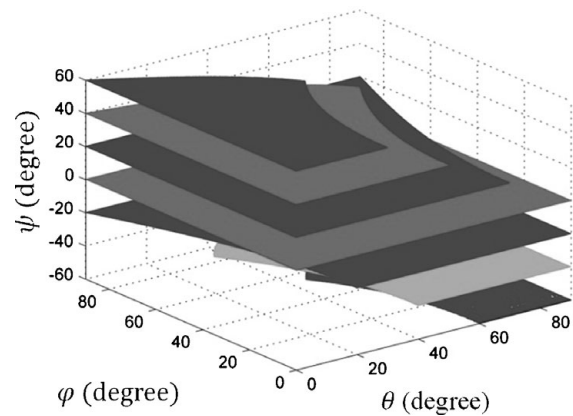


Fig. 11. Volumetric workspace in  $\theta$ - $\phi$ - $\psi$  space for the isotropic design.

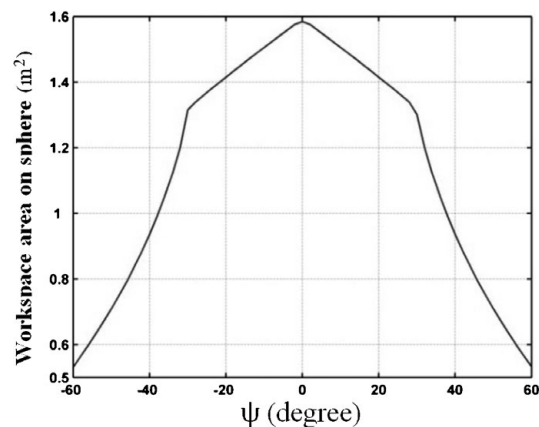


Fig. 12. Workspace area on sphere for the isotropic design vs.  $\psi$ .

analysis, a problem with a low condition number is said to be well-conditioned, while a problem with a high condition number is said to be ill-conditioned. When applied to manipulator Jacobian matrix, condition number will give a

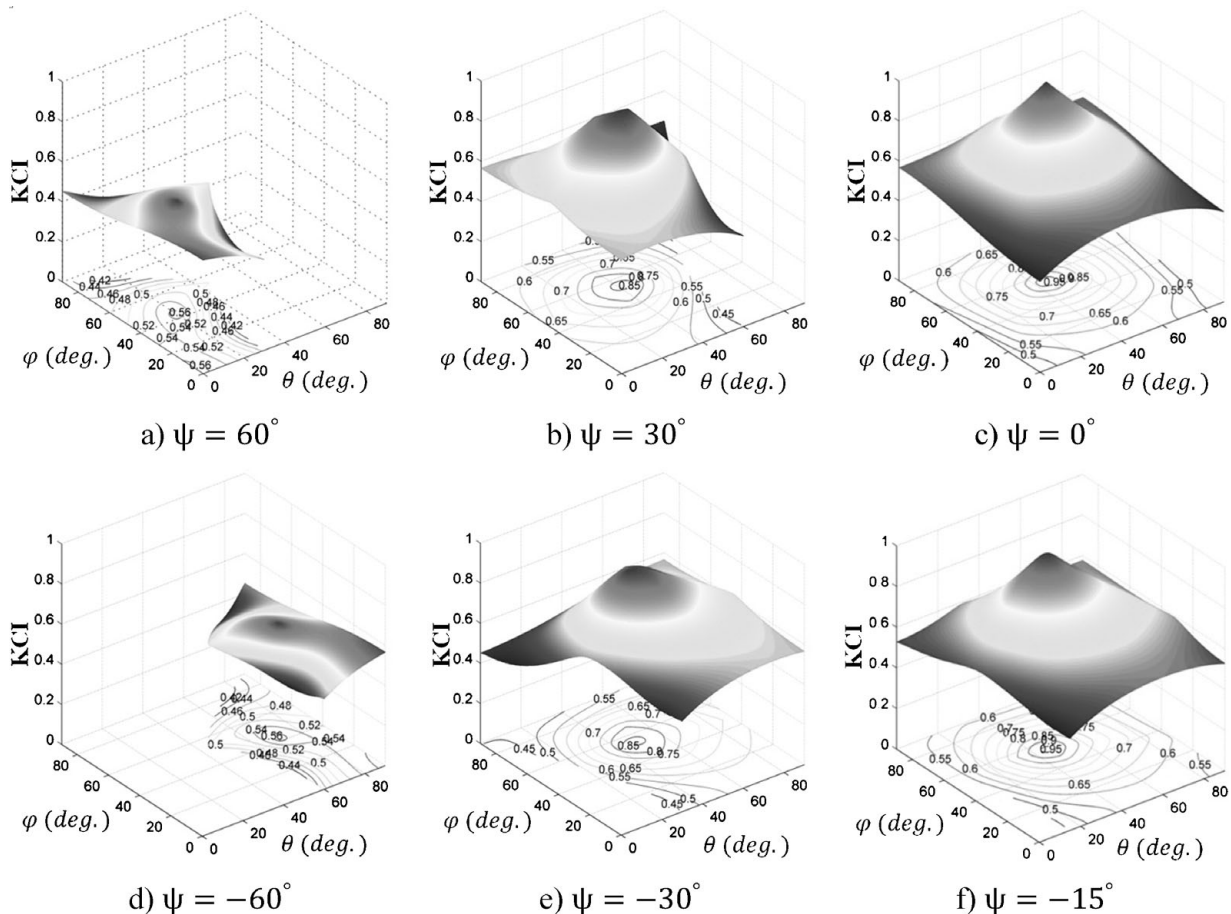


Fig. 13. KCI of the SST manipulator on sphere for different  $\psi$ .

measure of accuracy of the Cartesian velocity of the end-effector. It also provides a measure of accuracy of static load acting on the end-effector. The condition number can also be used to evaluate the dexterity of a manipulator.<sup>34</sup> It should be noted that the use of condition number for robot with mixed type of degrees of freedom (translations and rotations) is problematic.<sup>16,35</sup> However, the SST parallel manipulator has only rotational degrees of freedom and is not a mixed type. Therefore, we can use condition number as measure of accuracy. The condition number of Jacobian matrix can be written as

$$\kappa_{\mathbf{J}} = \frac{\sigma_{\mathbf{J},\max}}{\sigma_{\mathbf{J},\min}}, \quad (22)$$

where,  $\sigma_{\mathbf{J},\max}$  and  $\sigma_{\mathbf{J},\min}$  represent the maximum and minimum singular values of Jacobian matrix, respectively.  $\kappa_{\mathbf{J}}$  can reach values from 1 to  $\infty$ . In order to bound  $\kappa_{\mathbf{J}}$ , one may consider its inverse value defined by  $\eta_{\mathbf{J}} = 1/\kappa_{\mathbf{J}}$ . The variable  $\eta_{\mathbf{J}}$  is defined as kinematics conditioning index (KCI) and ranges between 0 and 1 (i.e., singular and isotropic configurations, respectively). This performance index is plotted for different values of  $\psi$  in Fig. 13. As seen in these figures, for any value of  $\psi$  there exists a minimum and a maximum value for KCI. These maximum and minimum values of KCI versus angle  $\psi$  are shown in Figs. 14 and 15, respectively. Figure 14 shows maximum value of KCI, which is equal to 1, occurs at  $\psi = 0^*$ . This configuration represents the isotropic configuration of the SST manipulator. Figure 15

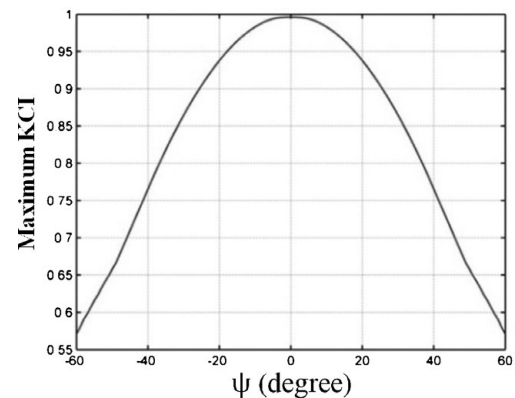


Fig. 14. Maximum KCI vs. angle  $\psi$ .

shows that minimum value of KCI occurs at  $\psi = 60^*$  and  $\psi = -60^*$ . This value is equal to 0.412. As stated earlier, KCI value equal to zero represents singular configuration. Since the minimum value of KCI is higher than zero, the isotropic design of the SST manipulator is free of singularity.

Since the kinematics index is dependent on the Jacobian matrix, it is a local property of the mechanism. KCI thus depends on the position and orientation of the end-effector as well as robot structure. Another performance index that covers the entire workspace is called global kinematics index (GCI). This type of index was introduced by Gosselin and Angeles.<sup>17</sup> This index is used to measure the global behavior of manipulator condition number. It computes the average of



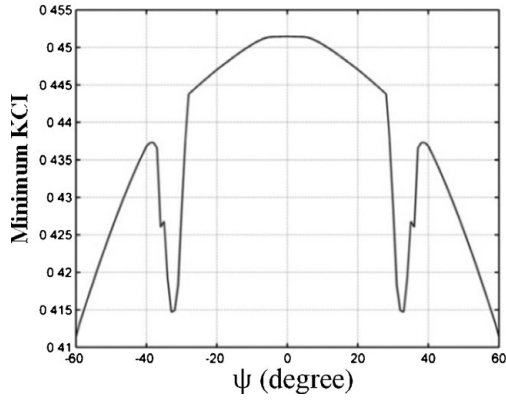

 Fig. 15. Minimum KCI vs. angle  $\psi$ .

Table I. Comparison maximum GCI.

SST manipulator	Spherical 3-RRR
0.67	0.52

the KCI throughout robot workspace. Therefore, GCI can be written as

$$GCI = \frac{\int_w \eta_J d_w}{\int_w d_w}, \quad (23)$$

where  $w$  is the manipulator's reachable workspace. For the SST manipulator, this value is equal to 0.67. This value is compared with the optimum design of another parallel manipulator<sup>13</sup> in Table I. Clearly the GCI of the SST manipulator is in "good" range compared with another SPM.

## 6. Stiffness Analysis

Stiffness (or rigidity) of a mechanism can be a primary consideration in the design of a parallel manipulator especially in applications involving large forces while requiring high accuracy. Stiffness measures resistance of an end-effector to small displacements when external forces or couples are applied to the end-effector. The stiffness of a parallel manipulator is primarily a function of:

- (1) Structure and material for each leg.
- (2) Joints stiffness.
- (3) Moving platform and base stiffness.
- (4) Topology of the manipulator.
- (5) Position and orientation of the end-effector.
- (6) Temperature, gap, preload, and other parameters.

The basic assumptions made for the stiffness analysis of the SST manipulator is as follows:

- (1) Negligible applied external forces compare to applied external torques. This assumption is made because the expected use of a spherical manipulator is to orient the tool.
- (2) Joints are frictionless.
- (3) Rigidity of the passive joints and base are assumed to be infinite.
- (4) Negligible weight for legs and MSS.
- (5) Remaining components are assumed to be flexible.
- (6) Strain energy due to shear forces is negligible.<sup>36</sup>

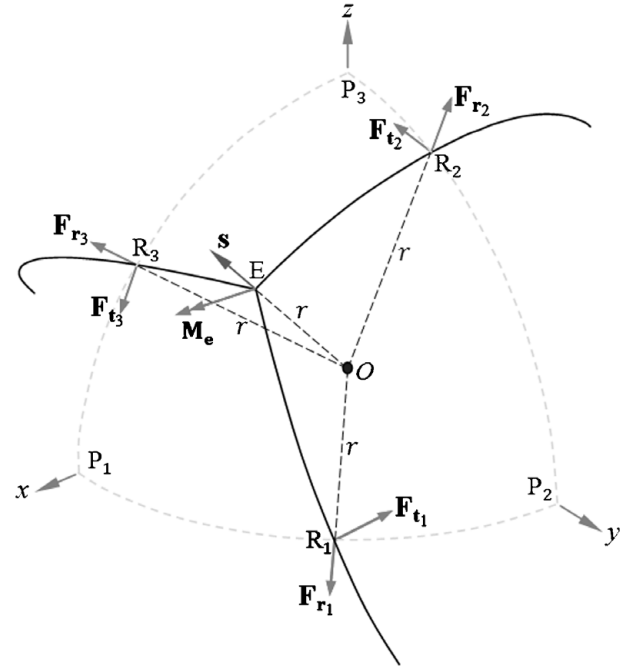


Fig. 16. Free body diagram (FBD) of MSS.

In the present paper, flexibility of the actuated joints, MSS, and all links between MSS and base will be considered. In order to obtain stiffness, we must first obtain forces acting on joints and links of the manipulator.

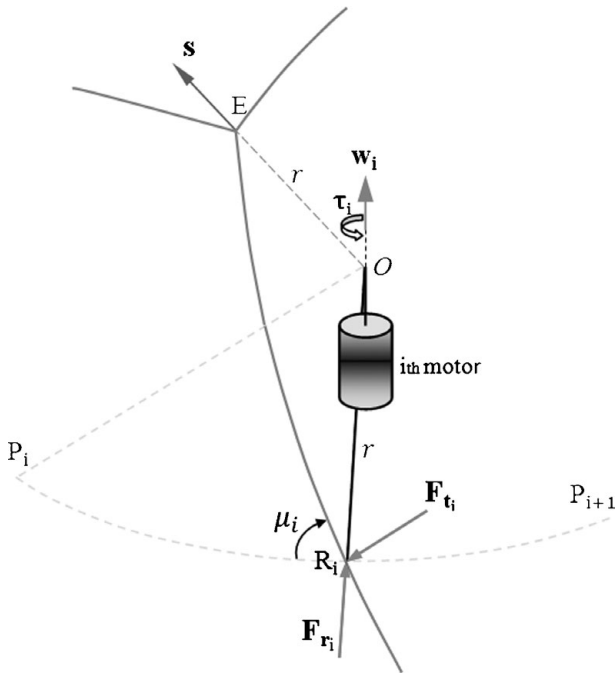
### 6.1. Force analysis

Before performing stiffness analysis, we must find relationship between the applied external torques on MSS (see Fig. 16) and the resultant joints forces. The aim of force analysis is to obtain analytical expressions for forces acting on joints while the manipulator is in equilibrium. These analytical expressions will allow us to calculate forces for all manipulator configurations. It is assumed that there is no friction in the system. The forces acting on the joints are found from the equilibrium equations written for each link and moving platform of the manipulator. Each leg of SST manipulator has three joints, an actuated revolute joint, a passive intermediate revolute joint, a curved prismatic passive joint as well as two links (see Fig. 1).

As stated before, the length of the link between passive intermediate revolute joint and passive curved prismatic joint is assumed to be negligible. Therefore, the reaction forces acting on passive curved prismatic joint are the same as those acting on passive intermediate revolute joint. The reaction forces  $\mathbf{F}_{t_i}$  and  $\mathbf{F}_{r_i}$  between MSS and  $i$ th curved prismatic passive joint are shown in Fig. 16. These reaction forces act through links attached to motors and are transferred to actuated joints (see Fig. 17). Therefore, we first obtain the reaction forces and next calculate torques applied to motors joints.

**6.1.1. Obtaining reaction forces.** As shown in Fig. 16, assume  $\mathbf{F}_{t_i}$  and  $\mathbf{F}_{r_i}$  are reaction force vectors between the MSS and  $i$ th curved prismatic passive joint. These forces can be written as

$$\mathbf{F}_{r_i} = F_{r_i} \mathbf{r}_i, \quad (24)$$

Fig. 17. Applied torque to  $i$ th motor.

$$\mathbf{F}_{t_i} = F_{t_i} \mathbf{t}_i, \quad (25)$$

where  $F_{r_i}$ ,  $F_{t_i}$  are values and  $\mathbf{r}_i$ ,  $\mathbf{t}_i$  are directions of reaction forces, respectively. For a given configuration of SST manipulator, direction of unit vectors  $\mathbf{r}_i$  and  $\mathbf{t}_i$  are determined by inverse kinematics problem. The relation between these forces and applied external torques on MSS may be written as

$$\sum \mathbf{M}_o = r(\mathbf{r}_1 \times \mathbf{t}_1)F_{t_1} + r(\mathbf{r}_2 \times \mathbf{t}_2)F_{t_2} + r(\mathbf{r}_3 \times \mathbf{t}_3)F_{t_3} + \mathbf{M}_e = \mathbf{0}, \quad (26)$$

$$\sum \mathbf{F} = \sum_{i=1}^3 (\mathbf{F}_{r_i} + \mathbf{F}_{t_i}) = \mathbf{r}_1 F_{r_1} + \mathbf{t}_1 F_{t_1} + \mathbf{r}_2 F_{r_2} + \mathbf{t}_2 F_{t_2} + \mathbf{r}_3 F_{r_3} + \mathbf{t}_3 F_{t_3} = \mathbf{0}, \quad (27)$$

where  $\mathbf{M}_e = [M_{ex} \ M_{ey} \ M_{ez}]^T$  is a vector of external torques applied to MSS. Using above equations,  $\mathbf{F}_t$  and  $\mathbf{F}_r$  can be written as function of  $\mathbf{M}_e$

$$\mathbf{F}_t = \mathbf{A} \mathbf{M}_e, \quad (28)$$

$$\mathbf{F}_r = \mathbf{B} \mathbf{M}_e, \quad (29)$$

where

$$\mathbf{F}_t = [F_{t_1} \ F_{t_2} \ F_{t_3}]^T, \quad (30)$$

$$\mathbf{F}_r = [F_{r_1} \ F_{r_2} \ F_{r_3}]^T, \quad (31)$$

and

$$\mathbf{A}_{3 \times 3} = -[r(\mathbf{r}_1 \times \mathbf{t}_1) \ r(\mathbf{r}_1 \times \mathbf{t}_1) \ r(\mathbf{r}_1 \times \mathbf{t}_1)]^{-1}, \quad (32)$$

$$\mathbf{B}_{3 \times 3} = -[\mathbf{r}_1 \ \mathbf{r}_2 \ \mathbf{r}_3]^{-1}[\mathbf{t}_1 \ \mathbf{t}_2 \ \mathbf{t}_3] \mathbf{A}. \quad (33)$$

Components of matrices  $\mathbf{A}$  and  $\mathbf{B}$  are called  $a_{ij}$  and  $b_{ij}$ , respectively.

6.1.2. Torque applied to motors joints. As shown in Fig. 17, if  $\mathbf{F}_{t_i}$  and  $\mathbf{F}_{r_i}$  are reaction force vectors then torque applied to  $i$ th motor can be written as

$$\tau_{m_i} = r F_{t_i} \sin \mu_i, \quad (34)$$

where  $\mu_i$  is angle between  $OP_i P_{i+1}$  and  $OER_i$  planes.

## 6.2. Stiffness matrix generation

Most previous stiffness analysis studies of parallel manipulators are performed using lumped model as well as assuming a rigid moving platform.<sup>25–26,37–39</sup> In this paper, we use continuous model as well as assuming flexible moving platform. Using strain energy approach, Castigliano's theorem, we obtain torsional stiffness of the SST manipulator. For this purpose, strain energy of all links, MSS as well as actuated joints are calculated. Strain energy of these elements are calculated using force analysis and inverse kinematics problem. When the motors are locked, we can write

$$U = U_s + U_l + U_m, \quad (35)$$

where  $U_s$  is strain energy of the MSS,  $U_l$  is strain energy of the three links,  $U_m$  is strain energy of the three motors and  $U$  is total strain energy of the SST manipulator. The values of strain energy depend on the applied external torques and manipulator configuration. These forces are assumed to act at point  $E$  since tool is attached to this point (see Fig. 16). If we assume motors are locked, the applied external torques will cause rotational deflection of the tool. The value of this rotation also depends on manipulator configuration. Therefore, in order to obtain torsional stiffness,  $\mathbf{K}$ , we can write

$$\mathbf{M}_e = \mathbf{K} \delta \boldsymbol{\varphi}, \quad (36)$$

where  $\delta \boldsymbol{\varphi}$  is called virtual rotation vector of the MSS center and  $\mathbf{M}_e$  is the external torques applied to center of MSS. Using Castigliano's theorem, we can obtain virtual rotation (rotational deflection) vector of MSS center as follows:

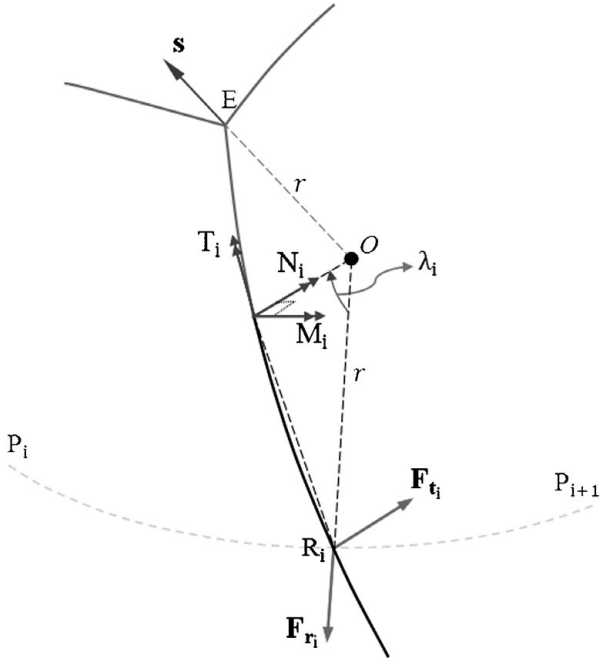
$$\begin{aligned} \delta \boldsymbol{\varphi} &= \frac{\partial U}{\partial \mathbf{M}_e} = \frac{\partial U_s}{\partial \mathbf{M}_e} + \frac{\partial U_l}{\partial \mathbf{M}_e} + \frac{\partial U_m}{\partial \mathbf{M}_e} = \delta \boldsymbol{\varphi}_s + \delta \boldsymbol{\varphi}_l + \delta \boldsymbol{\varphi}_m \\ &= (\mathbf{C}_s + \mathbf{C}_l + \mathbf{C}_m) \mathbf{M}_e = \mathbf{C} \mathbf{M}_e, \end{aligned} \quad (37)$$

where  $\delta \boldsymbol{\varphi}_s$  is virtual rotation vector due to flexibility of MSS,  $\delta \boldsymbol{\varphi}_l$  is virtual rotation vector due to flexibility of links and  $\delta \boldsymbol{\varphi}_m$  is virtual rotation vector due to flexibility of motors. Additionally,  $\mathbf{C}_s$ ,  $\mathbf{C}_l$ , and  $\mathbf{C}_m$  are compliance matrices of MSS, all links and motors, respectively.  $\mathbf{C}$  is compliance matrix of the manipulator. The above equation can be written as

$$\mathbf{M}_e = \mathbf{C}^{-1} \delta \boldsymbol{\varphi}. \quad (38)$$

Comparing Eqs. (36) and (38), we can write

$$\mathbf{K} = \mathbf{C}^{-1} \quad (39)$$

Fig. 18. FBD of  $i$ th branch of MSS.

In order to calculate matrix  $\mathbf{K}$ , we must calculate compliance matrix,  $\mathbf{C}$ , of the manipulator.

#### Calculation of compliance matrix for MSS, $C_s$

For this calculation, we must first obtain strain energy of MSS. The reaction forces  $F_{r_i}$ ,  $F_{t_i}$  result into two bending moments and a torsional moment in each branch of MSS (see Fig. 18).

We can write

$$M_i = r \| \mathbf{F}_{r_i} \| \sin \lambda_i \quad \text{for } i = 1, 2, 3, \quad (40)$$

$$N_i = r \| \mathbf{F}_{t_i} \| \sin \lambda_i \quad \text{for } i = 1, 2, 3, \quad (41)$$

$$T_i = 2r \| \mathbf{F}_{t_i} \| \sin^2(\lambda_i/2) \quad \text{for } i = 1, 2, 3, \quad (42)$$

where  $i$  represents one of the three MSS branches,  $\| \mathbf{F}_{r_i} \| = F_{r_i}$ ,  $\| \mathbf{F}_{t_i} \| = F_{t_i}$ ,  $M_i$  and  $N_i$  are bending moments and  $T_i$  is torsional moment. Using Eqs. (28) and (29), Eqs. (40–42) can be written as

$$M_i = r(b_{i1}M_{ex} + b_{i2}M_{ey} + b_{i3}M_{ez})\sin\lambda_i, \quad (43)$$

$$N_i = r(a_{i1}M_{ex} + a_{i2}M_{ey} + a_{i3}M_{ez})\sin\lambda_i, \quad (44)$$

$$T_i = 2r(a_{i1}M_{ex} + a_{i2}M_{ey} + a_{i3}M_{ez})\sin^2(\lambda_i/2), \quad (45)$$

where  $a_{ij}$  and  $b_{ij}$  are the components of matrices  $\mathbf{A}$  and  $\mathbf{B}$ , respectively. Strain energy of MSS,  $U_s$ , can now be written as follows:

$$U_s = \sum_{i=1}^3 \int_0^{\beta_i} \left( \frac{1}{2EI} (M_i^2 + N_i^2) + \frac{1}{2GJ} T_i^2 \right) (rd\lambda_i), \quad 0 \leq \lambda_i \leq \beta_i, \quad (46)$$

where  $E$  is elasticity modulus,  $G$  is elasticity shear modulus,  $I$  is centroidal moment of inertia and  $J$  is centroidal moment

of polar inertia. Using Castigliano's theorem, we must obtain partial derivation of Eq. (46) with respect to  $M_{ex}$ ,  $M_{ey}$ , and  $M_{ez}$ . This will result in

$$\delta\varphi_{sx} = \frac{\partial U_s}{\partial M_{ex}} = \sum_{i=1}^3 \int_0^{\beta_i} \left[ \frac{1}{EI} \left( M_i \frac{\partial M_i}{\partial M_{ex}} + N_i \frac{\partial N_i}{\partial M_{ex}} \right) + \frac{1}{GJ} \left( T_i \frac{\partial T_i}{\partial M_{ex}} \right) \right] (rd\lambda_i), \quad (47)$$

$$\delta\varphi_{sy} = \frac{\partial U_s}{\partial M_{ey}} = \sum_{i=1}^3 \int_0^{\beta_i} \left[ \frac{1}{EI} \left( M_i \frac{\partial M_i}{\partial M_{ey}} + N_i \frac{\partial N_i}{\partial M_{ey}} \right) + \frac{1}{GJ} \left( T_i \frac{\partial T_i}{\partial M_{ey}} \right) \right] (rd\lambda_i), \quad (48)$$

$$\delta\varphi_{sz} = \frac{\partial U_s}{\partial M_{ez}} = \sum_{i=1}^3 \int_0^{\beta_i} \left[ \frac{1}{EI} \left( M_i \frac{\partial M_i}{\partial M_{ez}} + N_i \frac{\partial N_i}{\partial M_{ez}} \right) + \frac{1}{GJ} \left( T_i \frac{\partial T_i}{\partial M_{ez}} \right) \right] (rd\lambda_i), \quad (49)$$

where  $\delta\varphi_s = [\delta\varphi_{sx} \quad \delta\varphi_{sy} \quad \delta\varphi_{sz}]^T$  is virtual rotation vector due to flexibility of MSS and  $\delta\varphi_{sx}$ ,  $\delta\varphi_{sy}$ , and  $\delta\varphi_{sz}$  are its x, y, and z components, in radians, respectively. By taking partial derivative of Eqs. (43–45), we can write:

$$\frac{\partial M_i}{\partial M_{ex}} = rb_{i1}\sin\lambda_i, \quad \frac{\partial M_i}{\partial M_{ey}} = rb_{i2}\sin\lambda_i, \quad \frac{\partial M_i}{\partial M_{ez}} = rb_{i3}\sin\lambda_i, \quad (50)$$

$$\frac{\partial N_i}{\partial M_{ex}} = ra_{i1}\sin\lambda_i, \quad \frac{\partial N_i}{\partial M_{ey}} = ra_{i2}\sin\lambda_i, \quad \frac{\partial N_i}{\partial M_{ez}} = ra_{i3}\sin\lambda_i, \quad (51)$$

$$\begin{aligned} \frac{\partial T_i}{\partial M_{ex}} &= 2ra_{i1}\sin^2(\lambda_i/2), \quad \frac{\partial T_i}{\partial M_{ey}} = 2ra_{i2}\sin^2(\lambda_i/2), \quad \frac{\partial T_i}{\partial M_{ez}} \\ &= 2ra_{i3}\sin^2(\lambda_i/2). \end{aligned} \quad (52)$$

Substituting above equations into Eqs. (47–49), will result

$$\begin{aligned} \delta\varphi_{sx} &= \frac{r^3}{EI} \sum_{i=1}^3 \int_0^{\beta_i} b_{i1}(b_{i1}M_{ex} + b_{i2}M_{ey} + b_{i3}M_{ez}) \\ &\quad \times \sin^2\lambda_i d\lambda_i + \frac{r^3}{EI} \sum_{i=1}^3 \int_0^{\beta_i} a_{i1}(a_{i1}M_{ex} + a_{i2}M_{ey} \\ &\quad + a_{i3}M_{ez})\sin^2\lambda_i d\lambda_i + \frac{4r^3}{GJ} \sum_{i=1}^3 \int_0^{\beta_i} a_{i1}(a_{i1}M_{ex} \\ &\quad + a_{i2}M_{ey} + a_{i3}M_{ez})\sin^4(\lambda_i/2) d\lambda_i, \end{aligned} \quad (53)$$

$$\begin{aligned} \delta\varphi_{sy} &= \frac{r^3}{EI} \sum_{i=1}^3 \int_0^{\beta_i} b_{i2}(b_{i1}M_{ex} + b_{i2}M_{ey} + b_{i3}M_{ez}) \\ &\quad \times \sin^2\lambda_i d\lambda_i + \frac{r^3}{EI} \sum_{i=1}^3 \int_0^{\beta_i} a_{i2}(a_{i1}M_{ex} + a_{i2}M_{ey} \\ &\quad + a_{i3}M_{ez})\sin^2\lambda_i d\lambda_i + \frac{4r^3}{GJ} \sum_{i=1}^3 \int_0^{\beta_i} a_{i2}(a_{i1}M_{ex} + a_{i2}M_{ey} \\ &\quad + a_{i3}M_{ez})\sin^4(\lambda_i/2) d\lambda_i, \end{aligned}$$

$$\begin{aligned}
& + a_{i3}M_{ez})\sin^2\lambda_i d\lambda_i + \frac{4r^3}{GJ} \sum_{i=1}^3 \int_0^{\beta_i} a_{i2}(a_{i1}M_{ex} \\
& + a_{i2}M_{ey} + a_{i3}M_{ez})\sin^4(\lambda_i/2)d\lambda_i, \quad (54)
\end{aligned}$$

$$\begin{aligned}
\delta\varphi_{sz} = & \frac{r^3}{EI} \sum_{i=1}^3 \int_0^{\beta_i} b_{i3}(b_{i1}M_{ex} + b_{i2}M_{ey} + b_{i3}M_{ez}) \\
& \times \sin^2\lambda_i d\lambda_i + \frac{r^3}{EI} \sum_{i=1}^3 \int_0^{\beta_i} a_{i3}(a_{i1}M_{ex} + a_{i2}M_{ey} \\
& + a_{i3}M_{ez})\sin^2\lambda_i d\lambda_i + \frac{4r^3}{GJ} \sum_{i=1}^3 \int_0^{\beta_i} a_{i3}(a_{i1}M_{ex} \\
& + a_{i2}M_{ey} + a_{i3}M_{ez})\sin^4\lambda_i d\lambda_i. \quad (55)
\end{aligned}$$

To calculate above integrations, we must obtain values of  $\beta_i$ . For any given orientation of MSS, the values of  $\beta_i$ , given by Eq. (16), are first determined from solving inverse kinematics problem. Substituting the values of  $\beta_i$  into Eqs. (53–55) and using MAPLE software to obtain the integration will result in

$$\begin{aligned}
\delta\varphi_{sx} = & \frac{r^3}{EI} \sum_{i=1}^3 b_{i1}(b_{i1}M_{ex} + b_{i2}M_{ey} + b_{i3}M_{ez}) \\
& \times (0.5\beta_i - 0.25\sin(2\beta_i)) \\
& + \frac{r^3}{EI} \sum_{i=1}^3 a_{i1}(a_{i1}M_{ex} + a_{i2}M_{ey} + a_{i3}M_{ez}) \\
& \times (0.5\beta_i - 0.25\sin(2\beta_i)) \\
& + \frac{4r^3}{GJ} \sum_{i=1}^3 a_{i1}(a_{i1}M_{ex} + a_{i2}M_{ey} + a_{i3}M_{ez}) \\
& \times (0.75\beta_i - 0.75\sin(2\beta_i) \\
& - 0.5\sin^3(\beta_i/2)\cos(\beta_i/2)), \quad (56)
\end{aligned}$$

$$\begin{aligned}
\delta\varphi_{sy} = & \frac{r^3}{EI} \sum_{i=1}^3 b_{i2}(b_{i1}M_{ex} + b_{i2}M_{ey} + b_{i3}M_{ez}) \\
& \times (0.5\beta_i - 0.25\sin(2\beta_i)) \\
& + \frac{r^3}{EI} \sum_{i=1}^3 a_{i2}(a_{i1}M_{ex} + a_{i2}M_{ey} + a_{i3}M_{ez}) \\
& \times (0.5\beta_i - 0.25\sin(2\beta_i)) \\
& + \frac{4r^3}{GJ} \sum_{i=1}^3 a_{i2}(a_{i1}M_{ex} + a_{i2}M_{ey} + a_{i3}M_{ez}) \\
& \times (0.75\beta_i - 0.75\sin(2\beta_i) \\
& - 0.5\sin^3(\beta_i/2)\cos(\beta_i/2)), \quad (57)
\end{aligned}$$

$$\begin{aligned}
\delta\varphi_{sz} = & \frac{r^3}{EI} \sum_{i=1}^3 b_{i3}(b_{i1}M_{ex} + b_{i2}M_{ey} + b_{i3}M_{ez}) \\
& \times (0.5\beta_i - 0.25\sin(2\beta_i)) \\
& + \frac{r^3}{EI} \sum_{i=1}^3 a_{i3}(a_{i1}M_{ex} + a_{i2}M_{ey} + a_{i3}M_{ez})
\end{aligned}$$

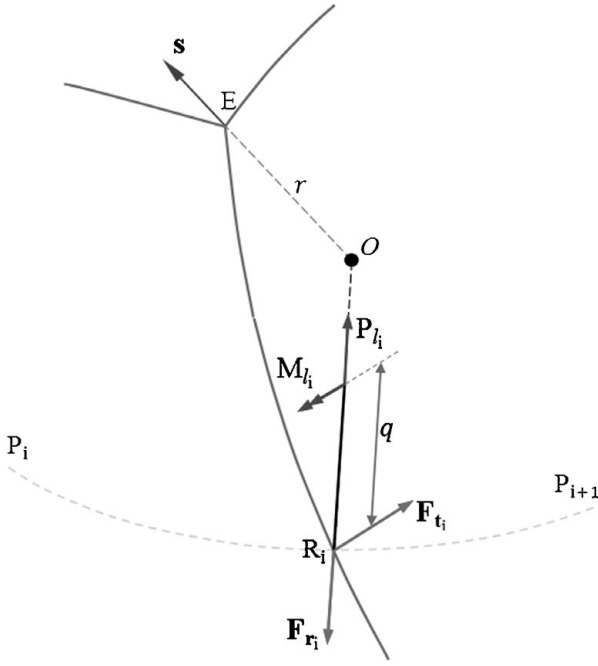
$$\begin{aligned}
& \times (0.5\beta_i - 0.25\sin(2\beta_i)) \\
& + \frac{4r^3}{GJ} \sum_{i=1}^3 a_{i3}(a_{i1}M_{ex} + a_{i2}M_{ey} + a_{i3}M_{ez}) \\
& \times (0.75\beta_i - 0.75\sin(2\beta_i) \\
& - 0.5\sin^3(\beta_i/2)\cos(\beta_i/2)). \quad (58)
\end{aligned}$$

By factoring external applied torques,  $M_{ex}$ ,  $M_{ey}$ , and  $M_{ez}$ , the above equations can be written as

$$\begin{aligned}
\delta\varphi_{sx} = & \left[ \begin{array}{c} \sum_{i=1}^3 \left( \frac{r^3}{EI} (b_{i1}^2 + a_{i1}^2) (0.5\beta_i - 0.25\sin(2\beta_i)) \right. \\ \left. + \frac{4r^3}{GJ} a_{i1}^2 (0.75\beta_i - 0.75\sin(2\beta_i) - 0.5\sin^3(\beta_i/2)\cos(\beta_i/2)) \right) \\ \sum_{i=1}^3 \left( \frac{r^3}{EI} (b_{i1}b_{i2} + a_{i1}a_{i2}) (0.5\beta_i - 0.25\sin(2\beta_i)) \right. \\ \left. + \frac{4r^3}{GJ} a_{i1}a_{i2} (0.75\beta_i - 0.75\sin(2\beta_i) - 0.5\sin^3(\beta_i/2)\cos(\beta_i/2)) \right) \\ \sum_{i=1}^3 \left( \frac{r^3}{EI} (b_{i1}b_{i3} + a_{i1}a_{i3}) (0.5\beta_i - 0.25\sin(2\beta_i)) \right. \\ \left. + \frac{4r^3}{GJ} a_{i1}a_{i3} (0.75\beta_i - 0.75\sin(2\beta_i) - 0.5\sin^3(\beta_i/2)\cos(\beta_i/2)) \right) \end{array} \right]^T \\
& \times \begin{bmatrix} M_{ex} \\ M_{ey} \\ M_{ez} \end{bmatrix} = \mathbf{C}_{sx} \mathbf{M}_e, \quad (59)
\end{aligned}$$

$$\begin{aligned}
\delta\varphi_{sy} = & \left[ \begin{array}{c} \sum_{i=1}^3 \left( \frac{r^3}{EI} (b_{i2}b_{i1} + a_{i2}a_{i1}) (0.5\beta_i - 0.25\sin(2\beta_i)) \right. \\ \left. + \frac{4r^3}{GJ} a_{i2}a_{i1} (0.75\beta_i - 0.75\sin(2\beta_i) - 0.5\sin^3(\beta_i/2)\cos(\beta_i/2)) \right) \\ \sum_{i=1}^3 \left( \frac{r^3}{EI} (b_{i2}^2 + a_{i2}^2) (0.5\beta_i - 0.25\sin(2\beta_i)) \right. \\ \left. + \frac{4r^3}{GJ} a_{i2}^2 (0.75\beta_i - 0.75\sin(2\beta_i) - 0.5\sin^3(\beta_i/2)\cos(\beta_i/2)) \right) \\ \sum_{i=1}^3 \left( \frac{r^3}{EI} (b_{i2}b_{i3} + a_{i2}a_{i3}) (0.5\beta_i - 0.25\sin(2\beta_i)) \right. \\ \left. + \frac{4r^3}{GJ} a_{i2}a_{i3} (0.75\beta_i - 0.75\sin(2\beta_i) - 0.5\sin^3(\beta_i/2)\cos(\beta_i/2)) \right) \end{array} \right]^T \\
& \times \begin{bmatrix} M_{ex} \\ M_{ey} \\ M_{ez} \end{bmatrix} = \mathbf{C}_{sz} \mathbf{M}_e, \quad (60)
\end{aligned}$$

$$\begin{aligned}
\delta\varphi_{sx} = & \left[ \begin{array}{c} \sum_{i=1}^3 \left( \frac{r^3}{EI} (b_{i3}b_{i1} + a_{i3}a_{i1}) (0.5\beta_i - 0.25\sin(2\beta_i)) \right. \\ \left. + \frac{4r^3}{GJ} a_{i3}a_{i1} (0.75\beta_i - 0.75\sin(2\beta_i) - 0.5\sin^3(\beta_i/2)\cos(\beta_i/2)) \right) \\ \sum_{i=1}^3 \left( \frac{r^3}{EI} (b_{i3}b_{i2} + a_{i3}a_{i2}) (0.5\beta_i - 0.25\sin(2\beta_i)) \right. \\ \left. + \frac{4r^3}{GJ} a_{i3}a_{i2} (0.75\beta_i - 0.75\sin(2\beta_i) - 0.5\sin^3(\beta_i/2)\cos(\beta_i/2)) \right) \\ \sum_{i=1}^3 \left( \frac{r^3}{EI} (b_{i3}^2 + a_{i3}^2) (0.5\beta_i - 0.25\sin(2\beta_i)) \right. \\ \left. + \frac{4r^3}{GJ} a_{i3}^2 (0.75\beta_i - 0.75\sin(2\beta_i) - 0.5\sin^3(\beta_i/2)\cos(\beta_i/2)) \right) \end{array} \right]^T \\
& \times \begin{bmatrix} M_{ex} \\ M_{ey} \\ M_{ez} \end{bmatrix} = \mathbf{C}_{sz} \mathbf{M}_e. \quad (61)
\end{aligned}$$


 Fig. 19. FBD of  $i$ th link.

Finally, we can write

$$\delta\boldsymbol{\varphi}_s = \begin{bmatrix} \delta\varphi_{sx} \\ \delta\varphi_{sy} \\ \delta\varphi_{sz} \end{bmatrix} = \begin{bmatrix} \mathbf{C}_{sx} \\ \mathbf{C}_{sy} \\ \mathbf{C}_{sz} \end{bmatrix}^T \mathbf{M}_e = \mathbf{C}_s \mathbf{M}_e, \quad (62)$$

where  $\mathbf{C}_s$  is compliance matrix due to flexibility of MSS.

*Calculation of compliance matrix for all links,  $C_l$*

As shown in Fig. 19, forces  $\mathbf{F}_{r_i}$  and  $\mathbf{F}_{t_i}$  are applied to end of each link. Forces  $\mathbf{F}_{r_i}$  and  $\mathbf{F}_{t_i}$  result in an axial force and a bending moment in each link, respectively. Therefore, we can write strain energy of links,  $U_l$ , as follow

$$U_l = \sum_{i=1}^3 \int_0^r \left( \frac{P_i^2}{2A_l E_l} + \frac{M_i^2}{2E_l I_l} \right) dq \quad 0 \leq q \leq r, \quad (63)$$

where  $M_i$  is bending moment in each link,  $P_i$  is axial force each link,  $A_l$  is cross section of link,  $E_l$  is modulus of elasticity,  $I_l$  is centroidal moment of inertia. Additionally,  $M_i$  and  $F_{r_i}$  can be written as

$$M_i = q F_{t_i} = q(a_{i1} M_{ex} + a_{i2} M_{ey} + a_{i3} M_{ez}) \quad 0 \leq q \leq r, \quad (64)$$

$$P_i = F_{r_i} = (b_{i1} M_{ex} + b_{i2} M_{ey} + b_{i3} M_{ez}), \quad (65)$$

where  $a_{ij}$  and  $b_{ij}$  are the components of the matrices  $\mathbf{A}$  and  $\mathbf{B}$ , respectively. Using Castigliano's theorem, we must obtain partial derivation of Eq. (63) with respect to  $M_{ex}$ ,  $M_{ey}$ , and  $M_{ez}$  will result

$$\delta\varphi_{lx} = \frac{\partial U_l}{\partial M_{ex}} = \sum_{i=1}^3 \int_0^r \left[ \frac{P_i}{A_l E_l} \frac{\partial P_i}{\partial M_{ex}} + \frac{1}{E_l I_l} \left( M_i \frac{\partial M_i}{\partial M_{ex}} \right) \right] dq \quad 0 \leq q \leq r, \quad (66)$$

$$\delta\varphi_{ly} = \frac{\partial U_l}{\partial M_{ey}} = \sum_{i=1}^3 \int_0^r \left[ \frac{P_i}{A_l E_l} \frac{\partial P_i}{\partial M_{ey}} + \frac{1}{E_l I_l} \left( M_i \frac{\partial M_i}{\partial M_{ey}} \right) \right] dq \quad 0 \leq q \leq r, \quad (67)$$

$$\delta\varphi_{lz} = \frac{\partial U_l}{\partial M_{ez}} = \sum_{i=1}^3 \int_0^r \left[ \frac{P_i}{A_l E_l} \frac{\partial P_i}{\partial M_{ez}} + \frac{1}{E_l I_l} \left( M_i \frac{\partial M_i}{\partial M_{ez}} \right) \right] dq \quad 0 \leq q \leq r, \quad (68)$$

where  $\delta\boldsymbol{\varphi}_l = [\delta\varphi_{lx} \ \delta\varphi_{ly} \ \delta\varphi_{lz}]^T$  is virtual rotation vector due to flexibility of links and  $\delta\varphi_{lx}$ ,  $\delta\varphi_{ly}$ , and  $\delta\varphi_{lz}$  are its x, y, and z components, in radians, respectively. By taking partial derivative of Eqs. (66)–(68), we can write

$$\frac{\partial M_i}{\partial M_{ex}} = q a_{i1}, \quad \frac{\partial M_i}{\partial M_{ey}} = q a_{i2}, \quad \frac{\partial M_i}{\partial M_{ez}} = q a_{i3}, \quad (69)$$

$$\frac{\partial P_i}{\partial M_{ex}} = b_{i1}, \quad \frac{\partial P_i}{\partial M_{ey}} = b_{i2}, \quad \frac{\partial P_i}{\partial M_{ez}} = b_{i3}. \quad (70)$$

Substituting above equations into Eqs. (66)–(68), will result

$$\delta\varphi_{lx} = \sum_{i=1}^3 \int_0^r \left[ \frac{1}{A_l E_l} b_{i1} (b_{i1} M_{ex} + b_{i2} M_{ey} + b_{i3} M_{ez}) + \frac{1}{E_l I_l} (q^2 a_{i1} (a_{i1} M_{ex} + a_{i2} M_{ey} + a_{i3} M_{ez})) \right] dq, \quad (71)$$

$$\delta\varphi_{ly} = \sum_{i=1}^3 \int_0^r \left[ \frac{1}{A_l E_l} b_{i2} (b_{i1} M_{ex} + b_{i2} M_{ey} + b_{i3} M_{ez}) + \frac{1}{E_l I_l} (q^2 a_{i2} (a_{i1} M_{ex} + a_{i2} M_{ey} + a_{i3} M_{ez})) \right] dq, \quad (72)$$

$$\delta\varphi_{lz} = \sum_{i=1}^3 \int_0^r \left[ \frac{1}{A_l E_l} b_{i3} (b_{i1} M_{ex} + b_{i2} M_{ey} + b_{i3} M_{ez}) + \frac{1}{E_l I_l} (q^2 a_{i3} (a_{i1} M_{ex} + a_{i2} M_{ey} + a_{i3} M_{ez})) \right] dq. \quad (73)$$

Integrating above equations and factoring external applied torques,  $M_{ex}$ ,  $M_{ey}$ , and  $M_{ez}$ , will result in

$$\delta\varphi_{lx} = \left[ \sum_{i=1}^3 \frac{r b_{i1}^2}{A_l E_l} + \frac{r^3 a_{i1}^2}{3 E_l I_l} \sum_{i=1}^3 \frac{r b_{i1} b_{i2}}{A_l E_l} + \frac{r^3 a_{i1} a_{i2}}{3 E_l I_l} \right. \\ \left. \times \sum_{i=1}^3 \frac{r b_{i1} b_{i3}}{A_l E_l} + \frac{r^3 a_{i1} a_{i3}}{3 E_l I_l} \right] \begin{bmatrix} M_{ex} \\ M_{ey} \\ M_{ez} \end{bmatrix} = \mathbf{C}_{lx} \mathbf{M}_e, \quad (74)$$

$$\delta\varphi_{ly} = \left[ \sum_{i=1}^3 \frac{r b_{i2} b_{i1}}{A_l E_l} + \frac{r^3 a_{i2} a_{i1}}{3 E_l I_l} \sum_{i=1}^3 \frac{r b_{i2}^2}{A_l E_l} + \frac{r^3 a_{i2}^2}{3 E_l I_l} \right. \\ \left. \times \sum_{i=1}^3 \frac{r b_{i2} b_{i3}}{A_l E_l} + \frac{r^3 a_{i2} a_{i3}}{3 E_l I_l} \right] \begin{bmatrix} M_{ex} \\ M_{ey} \\ M_{ez} \end{bmatrix} = \mathbf{C}_{ly} \mathbf{M}_e, \quad (75)$$

$$\delta\varphi_{lz} = \left[ \sum_{i=1}^3 \frac{rb_{i3}b_{i1}}{A_l E_l} + \frac{r^3 a_{i3} a_{i1}}{3E_l I_l} \sum_{i=1}^3 \frac{rb_{i3}b_{i2}}{A_l E_l} + \frac{r^3 a_{i3} a_{i2}}{3E_l I_l} \right. \\ \left. \times \sum_{i=1}^3 \frac{rb_{i3}^2}{A_l E_l} + \frac{r^3 a_{i3}^2}{3E_l I_l} \right] \begin{bmatrix} M_{ex} \\ M_{ey} \\ M_{ez} \end{bmatrix} = \mathbf{C}_{ly} \mathbf{M}_e, \quad (76)$$

Finally, we can write

$$\delta\boldsymbol{\varphi}_l = \begin{bmatrix} \delta\varphi_{lx} \\ \delta\varphi_{ly} \\ \delta\varphi_{lz} \end{bmatrix} = \begin{bmatrix} \mathbf{C}_{lx} \\ \mathbf{C}_{ly} \\ \mathbf{C}_{lz} \end{bmatrix}^T \mathbf{M}_e = \mathbf{C}_l \mathbf{M}_e, \quad (77)$$

where  $\mathbf{C}_l$  is compliance matrix due to flexibility of links.

*Calculation of compliance matrix for motors,  $\mathbf{C}_m$*

Finally, we can obtain strain energy of motors as follow

$$U_m = \sum_{i=1}^3 \left( \frac{1}{2} \tau_{m_i} \theta_{m_i} \right) = \sum_{i=1}^3 \left( \frac{\tau_{m_i}^2}{2k_{m_i}} \right), \quad (78)$$

where  $\tau_{m_i}$  is applied torque to  $i$ th motor,  $\theta_{m_i}$  is rotation of  $i$ th motor about axis  $\mathbf{w}_i$  when motor is locked and  $k_{m_i}$  is torsional stiffness of  $i$ th motor.

Substituting Eq. (34) in Eq. (78) and using Eq. (28), Eq. (78) can be written as

$$U_m = \sum_{i=1}^3 \left( \frac{(r F_{t_i} \sin(\mu_i))^2}{2k_{m_i}} \right) = \sum_{i=1}^3 \left( \frac{r^2 (1 - (\mathbf{w}_i^T \mathbf{t}_i)^2) F_{t_i}^2}{2k_{m_i}} \right) \\ = \sum_{i=1}^3 \left( \frac{r^2 (1 - (\mathbf{w}_i^T \mathbf{t}_i)^2) (a_{i1} M_{ex} + a_{i2} M_{ey} + a_{i3} M_{ez})^2}{2k_{m_i}} \right), \quad (79)$$

where  $a_{ij}$  are components of matrix  $\mathbf{A}$ . Using Castigliano's theorem, we must obtain partial derivation of Eq. (79) with respect to  $M_{ex}$ ,  $M_{ey}$ , and  $M_{ez}$ . This will result in

$$\delta\varphi_{mx} = \frac{\partial U_m}{\partial M_{ex}} \\ = \sum_{i=1}^3 \left( \frac{r^2 (1 - (\mathbf{w}_i^T \mathbf{t}_i)^2)}{k_{m_i}} a_{i1} (a_{i1} M_{ex} + a_{i2} M_{ey} + a_{i3} M_{ez}) \right), \quad (80)$$

$$\delta\varphi_{my} = \frac{\partial U_m}{\partial M_{ey}} \\ = \sum_{i=1}^3 \left( \frac{r^2 (1 - (\mathbf{w}_i^T \mathbf{t}_i)^2)}{k_{m_i}} a_{i2} (a_{i1} M_{ex} + a_{i2} M_{ey} + a_{i3} M_{ez}) \right), \quad (81)$$

$$\delta\varphi_{mz} = \frac{\partial U_m}{\partial M_{ez}} \\ = \sum_{i=1}^3 \left( \frac{r^2 (1 - (\mathbf{w}_i^T \mathbf{t}_i)^2)}{k_{m_i}} a_{i3} (a_{i1} M_{ex} + a_{i2} M_{ey} + a_{i3} M_{ez}) \right). \quad (82)$$

By factoring external applied torques,  $M_{ex}$ ,  $M_{ex}$ , and  $M_{ex}$ , the above equations can be written as

$$\delta\varphi_{mx} = \left[ \sum_{i=1}^3 \frac{r^2 (1 - (\mathbf{w}_i^T \mathbf{t}_i)^2) a_{i1}^2}{k_{m_i}} \sum_{i=1}^3 \frac{r^2 (1 - (\mathbf{w}_i^T \mathbf{t}_i)^2) a_{i1} a_{i2}}{k_{m_i}} \right. \\ \left. \times \sum_{i=1}^3 \frac{r^2 (1 - (\mathbf{w}_i^T \mathbf{t}_i)^2) a_{i1} a_{i3}}{k_{m_i}} \right] \begin{bmatrix} M_{ex} \\ M_{ey} \\ M_{ez} \end{bmatrix} = \mathbf{C}_{mx} \mathbf{M}_e, \quad (83)$$

$$\delta\varphi_{my} = \left[ \sum_{i=1}^3 \frac{r^2 (1 - (\mathbf{w}_i^T \mathbf{t}_i)^2) a_{i2} a_{i1}}{k_{m_i}} \sum_{i=1}^3 \frac{r^2 (1 - (\mathbf{w}_i^T \mathbf{t}_i)^2) a_{i2}^2}{k_{m_i}} \right. \\ \left. \times \sum_{i=1}^3 \frac{r^2 (1 - (\mathbf{w}_i^T \mathbf{t}_i)^2) a_{i2} a_{i3}}{k_{m_i}} \right] \begin{bmatrix} M_{ex} \\ M_{ey} \\ M_{ez} \end{bmatrix} = \mathbf{C}_{my} \mathbf{M}_e, \quad (84)$$

$$\delta\varphi_{mz} = \left[ \sum_{i=1}^3 \frac{r^2 (1 - (\mathbf{w}_i^T \mathbf{t}_i)^2) a_{i3} a_{i1}}{k_{m_i}} \sum_{i=1}^3 \frac{r^2 (1 - (\mathbf{w}_i^T \mathbf{t}_i)^2) a_{i3} a_{i2}}{k_{m_i}} \right. \\ \left. \times \sum_{i=1}^3 \frac{r^2 (1 - (\mathbf{w}_i^T \mathbf{t}_i)^2) a_{i3}^2}{k_{m_i}} \right] \begin{bmatrix} M_{ex} \\ M_{ey} \\ M_{ez} \end{bmatrix} = \mathbf{C}_{mz} \mathbf{M}_e. \quad (85)$$

Therefore, we can assemble Eqs. (83–85) as follow

$$\delta\boldsymbol{\varphi}_m = \begin{bmatrix} \delta\varphi_{mx} \\ \delta\varphi_{my} \\ \delta\varphi_{mz} \end{bmatrix} = \begin{bmatrix} \mathbf{C}_{mx} \\ \mathbf{C}_{my} \\ \mathbf{C}_{mz} \end{bmatrix} \mathbf{M}_e = \mathbf{C}_m \mathbf{M}_e, \quad (86)$$

where  $\mathbf{C}_m$  is compliance matrix due to flexibility of motors.

This completes mathematical calculation of SST manipulator stiffness. The correctness of the mathematical stiffness model is next verified using a commercial finite element analysis package. Therefore, a finite element analysis model is next considered.

## 7. Finite Element Analysis (FEA) Model

An FEA model is used to simulate the physical structure and compare its results with the stiffness predicted by the mathematical model developed in the previous section.

### 7.1. Description of the FEA model

A finite element commercial software is used to develop finite element model of SST manipulator. Three element types are used in this modeling: BEAM189, MPC184 and COMBIN14. In this model, the number of elements and nodes are 378 and 727, respectively. Structural members are assumed to be the end-effector (MSS) and the motor links. These members are modeled by BEAM189 element type. This element is based on Timoshenko beam theory. In this modeling, the cross-section of the structural members are assumed to be circular. Diameter of this circle is 0.02 meters.

The radius of sphere on which MSS travels is assumed to be one meter. The structural members are assumed to be made of steel with module of elasticity and Poisson's ratio of 207 GPa and 0.27, respectively.

Each leg of SST manipulator has two passive and one active joint. The two passive joints, assumed to be rigid, connect the flexible MSS to the flexible motor link and produce simple kinematic constraint. This constraint allows motion transmission between the two flexible members. To define this constraint, multipoint constraint element, MPC184, is used. For this purpose, two nodes are selected, one attached to MSS and the other attached to the motor link. The two nodes coincide with each other but are not merged. Since, the intermediate revolute and curved prismatic joints are assumed to be rigid, then the MPC184 element that is also a rigid element is a good choice to model the revolute and curved prismatic joints.

The motor of SST manipulator are not completely rigid. Therefore, the motors are modeled by a torsional spring about motor's revolution axis. For this purpose, a torsional spring element, COMBIN14, is selected to simulate stiffness of motor. In this model, torsional spring constant is assumed as  $2 \times 10^6$  Nm/rad. Next, using the selected elements discussed above, SST manipulator is modeled.

### 7.2. Case studies description and results

In this subsection, three different orientations for MSS are considered. These three case studies are used to compare the mathematical model developed in Section 6 with FEA model. For all three cases, the external torque applied to the center of MSS is assumed to act about vector  $\mathbf{s}$ . Therefore, we can write

$$\mathbf{M}_e = [M_{ex} \quad M_{ey} \quad M_{ez}]^T = 10\mathbf{s} \text{ Nm.}$$

Note that the unit vector  $\mathbf{s}$  shows the direction about which external torque is applied. To obtain rotational deflection of end-effector, rotation of the node that coincides with center of MSS (point  $E$ ) is considered. Rotation of this node depends on external torque  $\mathbf{M}_e$  and orientation of MSS. Rotations of this node for three different case studies are computed by finite element commercial software and compared with the mathematical model (see Table II). These results verify the correctness of the mathematical model. Also, you can see deformed and un-deformed shape of FEM model for case 1 in figure 20.

## 8. Stiffness Evaluation

For a given SST manipulator structure, stiffness is a function of its configuration. This is because the effective length and

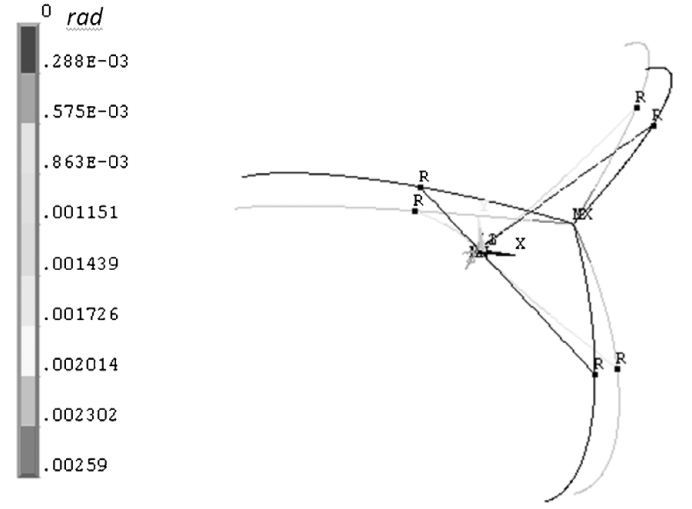


Fig. 20. Deformed and un-deformed shape of FEM model for case 1.

orientation of branches are different for the given configuration. For this reason, the KSI, used in ref. [40] and others, is considered. This index,  $\kappa_{\mathbf{K}}$ , is computed in a similar fashion to KCI by using condition number of stiffness matrix as

$$\kappa_{\mathbf{K}} = \frac{\sigma_{\mathbf{K},\max}}{\sigma_{\mathbf{K},\min}}, \quad (87)$$

where,  $\sigma_{\mathbf{K},\max}$  and  $\sigma_{\mathbf{K},\min}$  represent the maximum and minimum singular values of stiffness matrix,  $\mathbf{K}$ , respectively. Since  $\kappa_{\mathbf{K}}$  can reach values from 1 to  $\infty$ ,  $\eta_{\mathbf{K}} = 1/\kappa_{\mathbf{K}}$  is used which bounds stiffness index between 0 and 1. This performance index is called KSI and is plotted for different values of  $\psi$  in Fig. 20 Fig. 21. Also, the maximum value of KSI versus angle  $\psi$  is shown in Fig. 22. This figure demonstrates that maximum KSI occurs at  $\psi = 0^\circ$ .

In the present work, another performance measure of stiffness, namely, GSI, that depicts the uniformity of stiffness within the whole workspace, used in ref. [40], is considered. The GSI is defined as inverse of condition number of stiffness matrix,  $\eta_{\mathbf{K}}$ , integrated over the reachable workspace and divided by the volume of the workspace. Therefore, GSI can be written as

$$\text{GSI} = \frac{\int_w \eta_{\mathbf{K}} dw}{\int_w dw}. \quad (88)$$

Where GSI is used to measure global behavior of manipulator stiffness index and  $w$  is the manipulator's reachable workspace. For SST manipulator, the value of GSI is equal to 0.47.

Table II. Comparison results of FEM model with mathematical model.

Case study	Orientation of MSS			FEM model				Mathematical model			
	$\theta$ (rad)	$\varphi$ (rad)	$\psi$ (rad)	$\delta\varphi_x$ (rad)	$\delta\varphi_y$ (rad)	$\delta\varphi_z$ (rad)	$\ \delta\boldsymbol{\varphi}\ $ (rad)	$\delta\varphi_x$ (rad)	$\delta\varphi_y$ (rad)	$\delta\varphi_z$ (rad)	$\ \delta\boldsymbol{\varphi}\ $ (rad)
1	$\frac{\pi}{4}$	$\frac{54.74\pi}{180}$	0	0.00149	0.00149	0.00149	0.00258	0.0015	0.0015	0.0015	0.00259
2	$\frac{\pi}{4}$	$\frac{44.74\pi}{180}$	0	0.0013	0.0013	0.0020	0.00272	0.00121	0.00121	0.0021	0.00271
3	$\frac{\pi}{4}$	$\frac{54.7\pi}{180}$	$\frac{\pi}{6}$	0.00129	0.00129	0.00129	0.00223	0.0013	0.0013	0.0013	0.00225

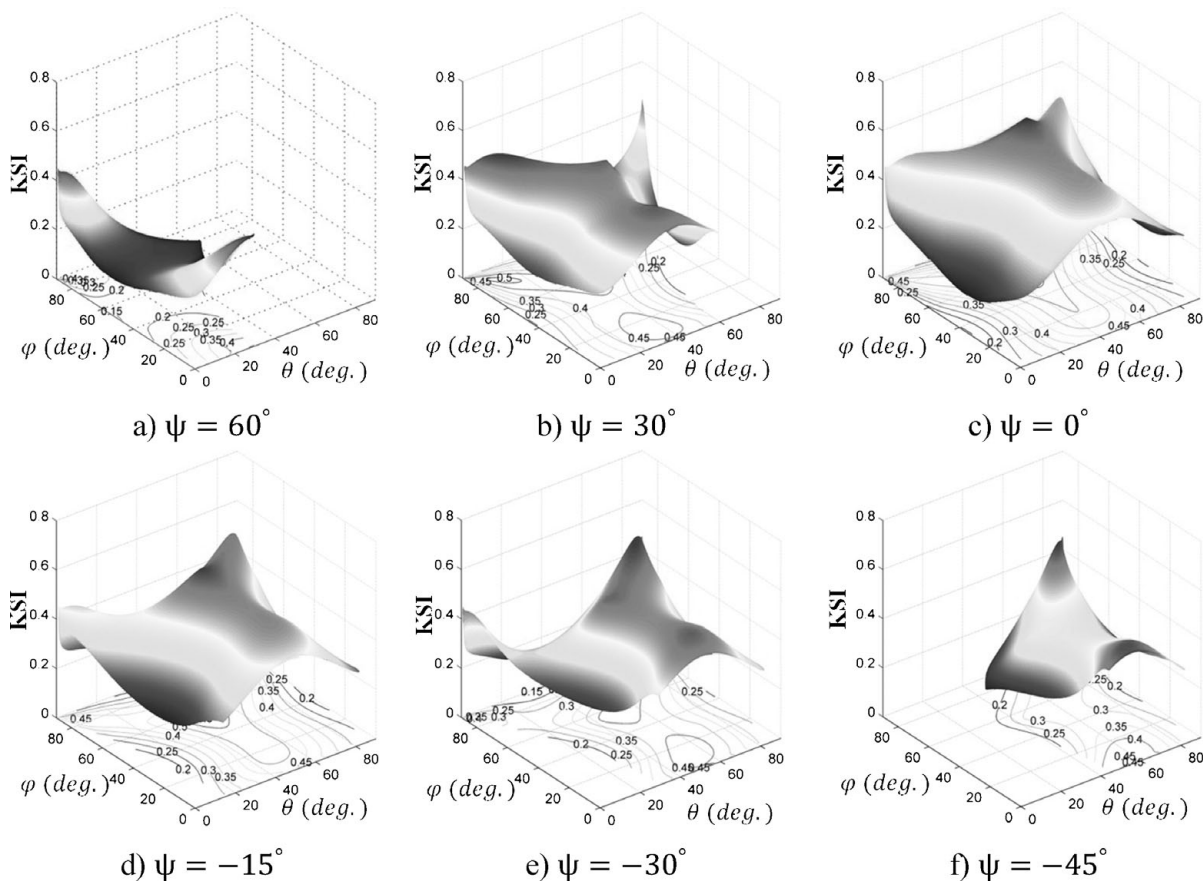


Fig. 21. KSI of SST manipulator on sphere for different  $\psi$ .

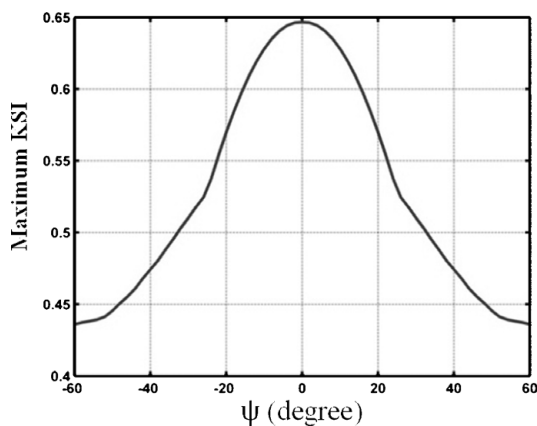


Fig. 22. Maximum KSI vs. angle  $\psi$ .

It should be noted that values of GSI and KSI are both functions of material and structural properties of links and MSS as well as torsional stiffness of the motors. By choosing proper values of these parameters, designers can design a robot with desired GSI with minimum variation.

## 9. Conclusion

The need for a mechanism capable of accurately orienting a heavy payload is apparent. This has motivated us to design the SST manipulator. Previous studies regarding parallel manipulators have assumed rigid moving platform. However, the need to carry heavy payload has motivated us to assume

a flexible moving platform. Therefore, in the present paper, inverse kinematics problem, workspace analysis, accuracy, and stiffness analysis of SST manipulator, a 3-RRP SPM, were studied. To perform these analyses, isotropic design was selected. Equivalent angle-axis representation was used and a closed form solution was obtained for the inverse kinematics problem. Workspace analysis was presented and it was shown that SST manipulator has a relatively large workspace. Next, accuracy analysis was performed using inverse kinematics, Jacobian matrices, and workspace analyses. Two accuracy performance measures, KCI and GCI were calculated. The GCI of SST manipulator was compared with the 3-RRR SPM. Results indicated that GCI of SST manipulator is in “good” range. Stiffness analysis was next presented. A continuous method based on strain energy and Castigliano’s theorem was used for stiffness analysis. The moving platform (MSS), all links and motors were assumed flexible and torsional stiffness matrix of SST manipulator was obtained. A commercial FEM package was used to model the SST manipulator. Results of finite element analysis were compared with mathematical model and was shown that the two models closely agree. Lastly, using mathematical model, stiffness evaluation of SST manipulator was performed and KSI and GSI indices were evaluated.

## References

1. J. Enferadi and A. A. Tootoonchi, “A novel spherical parallel manipulator: Forward position problem, singularity analysis and isotropic design,” *Robotica* **27**, 663–676 (2009).



2. R. Di Gregorio, "The 3-RRS wrist: A new, simple and non-overconstrained spherical parallel manipulator," *J. Mech. Des.* **126**, 850–855 (2004).
3. D. Chablat and J. Angeles, "The Computation of all 4R serial spherical wrists with an isotropic architecture," *J. Mech. Des.* **125**(2), 275–280 (2003).
4. J. M. Wiitala and M. M. Stanisic, "Design of an overconstrained and dexterous spherical wrist," *J. Mech. Des.* **122**(3), 347–353 (2000).
5. R. Di Gregorio, "A new family of spherical parallel manipulators," *Robotica* (20), 353–358 (2002).
6. K. C. Gupta, "On the nature of robot workspace," *Int. J. Robot. Res.* **5**(2), 112–121 (1985).
7. C. M. Gosselin and M. Jean, "Determination of the workspace of planar parallel manipulators with joint limits," *Robot. Auton. Syst.* **17**, 129–138 (1996).
8. C. A. Klein and B. E. Blaho, "Dexterity measures for the design and control of kinematically redundant manipulators," *Int. J. Robot. Res.* **6**, 72–82 (1987).
9. C. M. Gosselin, "The optimum design of robotic manipulators using dexterity indices," *Robot. Auton. Syst.* **9**, 213–226 (1992).
10. F. Gao, F. Guy and W. A. Gruver, "Criteria Based Analysis and Design of Three Degree-of-Freedom Planar Robotic Manipulators," *IEEE International Conference on Robotics and Automation*, New Mexico (1997) pp. 468–473.
11. F. Gao, X. J. Liu and W. A. Gruver, "The Global Conditioning Index in the Solution Space of Two Degree-of-Freedom Planar Parallel Manipulators," *IEEE SMC'95*, Vancouver, BC, Canada (1995) pp. 4055–4058.
12. F. Gao, X. J. Liu and W. A. Gruver, "Performance evaluation of two degrees-of-freedom planar parallel robots," *Mech. Mach. Theory* **33**(2), 661–668 (1998).
13. C. M. Gosselin, Kinematic Analysis, Optimization and Programming of Parallel Robotic Manipulators *Ph.D. thesis* (Montreal, Quebec, Canada: McGill University, 1988).
14. C. M. Gosselin, "Stiffness map for parallel manipulators," *IEEE Trans. Robot. Autom.* **6**(3), 377–382 (1990).
15. M. Arsenaault and R. Boudreau, "Synthesis of planar parallel mechanisms while considering workspace, dexterity, stiffness and singularity avoidance," *J. Mech. Des.* **128**(1), 69–78 (2006).
16. J. P. Merlet, "Jacobian, manipulability, condition number, and accuracy of parallel robots," *J. Mech. Des.* **128**(1), 199–205 (2006).
17. C. M. Gosselin and J. Angeles, "A global performance index for the kinematic optimization of robotic manipulators," *J. Mech. Des.* **113**(3), 220–226 (1991).
18. J. P. Merlet, *Les Robots Parallèles*, 2nd ed. (Hermès, Paris, France, 1997).
19. M. Ceccarelli and G. Carbone, "A stiffness analysis for CaPaMan (CassinoParallel Manipulator)," *Mech. Mach. Theory* **37**(5), 427–439 (2002).
20. T. Huang, X. Zhao and D. J. Whitehouse, "Stiffness estimation of a tripod-based parallel kinematic machine," *IEEE Trans. Robot. Autom.* **18**(1), 50–58 (2002).
21. S. Bhattacharyya, H. Hatwal and A. Ghosh, "On the optimum design of Stewart platform type parallel manipulators," *Robotica* **13**(2), 133–140 (1995).
22. B. S. El-Khasawneh and P. M. Ferreira, "Computation of stiffness and stiffness bounds for parallel link manipulators," *Int. J. Mach. Tools Manuf.* **39**(2), 321–342 (1999).
23. L. W. Tsai and S. Joshi, "Kinematics analysis of 3-DOF position mechanisms for use in hybrid kinematic machines," *J. Mech. Des.* **124**(2), 245–253 (2002).
24. X. J. Liu, Z. L. Jin and F. Gao, "Optimum design of 3-DOF spherical parallel manipulators with respect to the conditioning and stiffness indices," *Mech. Mach. Theory* **35**(9), 1257–1267 (2000).
25. C. M. Gosselin and D. Zhang, "Stiffness analysis of parallel mechanisms using a lumped model," *Int. J. Rob. Autom.* **17**(1), 17–27 (2002).
26. F. Majou, C. M. Gosselin, P. Wenger and D. Chablat, "Parametric stiffness analysis of the Orthoglide," *Mech. and Mach. Theory* **42**, 296–311 (2007).
27. [Online]. Available <http://www.rollonbearings.com/linearalraais.html>
28. J. Craig, *Introduction to Robotics: Mechanics and Control* (Addison-Wesley, 1989).
29. J. Angeles, *Fundamentals of Robotic Mechanical Systems: Theory, Methods and Algorithms*, 2nd ed. (Springer, 2002).
30. C. W. Wampler, "On a rigid body subject to point-plane constraints," *J. Mech. Des.* **128**, 151–158 (2006).
31. V. Kumar, "Characterization of workspaces of parallel manipulators," *J. Mech. Des.* **114**(3), 368–375 (1992).
32. J. P. Merlet, C. M. Gosselin and N. Mouly, "Workspaces of planar parallel manipulators," *Mech. Mach. Theory* **33**, 7–20 (1998).
33. G. Strang, *Linear Algebra and its Application* (Academic Press, New York, 1976).
34. J. K. Salisbury and J. Graig, "Articulated hands: Force control and kinematic issues," *Int. J. Robot. Res.* **1**(1), 4–17 (1982).
35. A. Yu, I. A. Bonev and P. Zsombor-Murray, "Geometric approach to the accuracy analysis of a class of 3-DOF planar parallel robots," *Mech. Mach. Theory* **43**, 364–375 (2008).
36. F. P. Beer and E. R. Johnston, *Mechanics of Materials* (McGraw-Hill, 1988).
37. Q. Xu and Y. Li, "An investigation on mobility and stiffness of a 3-DOF translational parallel manipulator via screw theory," *Robot. Comput. Integr. Manuf.* **24**, 402–414 (2008).
38. Y. Li and Q. Xu, "Stiffness analysis for a 3-PUU parallel kinematic machine," *Mech. Mach. Theory* **43**, 186–200 (2008).
39. H. K. Jung, C. D. Crane and R. G. Roberts, "Stiffness mapping of compliant parallel mechanisms in a serial arrangement," *Mech. and Mach. Theory* **43**, 271–284 (2008).
40. X.-J. Liu, X. Tang and J. Wang, "A Novel 2-DOF Parallel Mechanism based Design of a New 5-Axis Hybrid Machine Tool," *IEEE International Conference on Robotics and Automation*, Taipei, Taiwan (2003), pp. 3990–3995.